공학박사학위논문

소금쟁이 모사
초소형 수면 도약 로봇

Water Strider Inspired
At-scale Water Jumping Robot

2014 년 8 월

서울대학교 대학원

기계항공공학부

고 제 성

소금쟁이 모사
초소형 수면 도약 로봇

Water Strider Inspired
At-scale Water Jumping Robot

지도교수 조 규 진

이 논문을 공학박사 학위논문으로 제출함
2014 년 6 월

서울대학교 대학원
기계항공공학부
고 제 성

고제성의 공학박사 학위논문을 인준함
2014 년 6 월

위 원 장 주 종 남 (인)

부위원장 조 규 진 (인)

위 원 김 호 영 (인)

위 원 이 상 엽 (인)

위 원 박 용 재 (인)

학위논문 원문제공 서비스에 대한 동의서

본인의 학위논문에 대하여 서울대학교가 아래와 같이 학위논문 저작물을 제공하는 것에 동의합니다.

1. 동의사항

① 본인의 논문을 보존이나 인터넷 등을 통한 온라인 서비스 목적으로 복제할 경우 저작물의 내용을 변경하지 않는 범위 내에서의 복제를 허용합니다.

② 본인의 논문을 디지털화하여 인터넷 등 정보통신망을 통한 논문의 일부 또는 전부의 복제.배포 및 전송 시 무료로 제공하는 것에 동의합니다.

2. 개인(저작자)의 의무

본 논문의 저작권을 타인에게 양도하거나 또는 출판을 허락하는 등 동의 내용을 변경하고자 할 때는 소속대학(원)에 공개의 유보 또는 해지를 즉시 통보하겠습니다.

3. 서울대학교의 의무

① 서울대학교는 본 논문을 외부에 제공할 경우 저작권 보호장치(DRM)를 사용하여야 합니다.

② 서울대학교는 본 논문에 대한 공개의 유보나 해지 신청 시 즉시 처리해야 합니다.

논문제목 : Water Strider Inspired At-scale Water Jumping Robot

학위구분 : 석사 ☐ · 박사 ☑
학 과 : 기계항공공학부
학 번 : 2008-22866
연 락 처 : 010-9343-8806
저 작 자 : 고 제 성 (인)

제 출 일 : 2014 년 7 월 30 일

서울대학교총장 귀하

Abstract

Water Strider Inspired At-scale Water Jumping Robot

Je-Sung Koh
School of Mechanical and Aerospace Engineering
The Graduate School
Seoul National University

Water striders shows remarkable movement on the water surface. They can walk and slide freely, and sometimes jump and leap out of the water surfaces. These extreme locomotion inspires the robotic researchers to break the mobility limitation of the robots by developing the robot that is capable of walking and jumping on water.

To build the robotic water striders, the hydrodynamics acting on the driving legs with the water surface is analyzed theoretically to abstract the principles and criteria for the robot design. We found that the curvature force of the water surface is the largest and dominant hydrodynamic force in jumping on water of the water striders. The design criteria is established for the robot to obtain the maximum curvature forces from the water surface and not to break the water surface which causes reducing the reaction force and the momentum transfer to the robotic water striders significantly. The criteria is that the reaction force per submerged leg length should be below the maximum water surface curvature force generated by the surface tension of water.

The dimensions of the water striders is around of 2~3 cm in body length,

3~5 cm in leg length and weight of 50mg. It is much smaller and lighter than the conventional robotic systems and machines. The robotic water striders weigh about 1/6 of a single 3mm nut which is basic element of conventional machines. The smart composite microstructures (SCM) process is employed to build the small scale robotic structures. The precision laser machining and laminating process with fiber reinforced composite materials enable to fabricate millimeter scale articulated robotic structures with minimum friction loss in working. The shape memory alloy (SMA) actuator is embedded on the robot as an artificial muscle of the robot.

To satisfy the design criteria with maximum momentum transfer, the flea inspired catapult mechanism, called the torque reversal catapult, is employed to design the controllable jumping mechanism. The unique force profile of the torque reversal catapult mechanism enables to maximize the momentum transfer with the low reaction force. Moreover, the robot structure is simplified dramatically by applying the passive triggering components.

Finally, the robotic water strider prototypes are built with 2 cm in body length, 3~5cm in leg length and around 55 mg in weight. The robots can be designed with various design parameters to change the jumping power of the robots to meet the design criteria. The results show that the robotic water strider jumps and leaps out of the water surface smoothly with the takeoff velocity of 1.5 m/s. If the robotic water strider satisfies the design criteria, the takeoff velocity on water and ground are almost same because the water surface generates enough forces that can endure the driving force of the legs. Water-

ground velocity ratio of the experimental results show how efficient the robot can jump on water compared with jumping on the ground. When the reaction force per submerged length exceed the maximum curvature force of the water surface, the takeoff velocity on water decrease rapidly compared with the jumping on the ground.

By developing the robotic water strider, the robot itself would be used as an environment surveillance robots. In addition, the enabling technologies expand the scale limitation in the wide spectrum of the robotics.

Keywords: Jumping on Water, Water strider robot, Shape Memory Alloy Actuator, Fiber Reinforce Composite, Surface tension, Micro robot

Student Number: 2008-22866

Nomenclature

F_d	form drag force
F_v	viscosity force
F_b	buoyancy
F_s	surface curvature force
F_i	added inertia
F_m	Marangoni force
ρ	density of water
U	speed of the leg
A	characteristic area of the leg
μ	viscosity of water
g	gravitational acceleration
h	depth of the leg from the free surface of water
γ	surface tension coefficient
w	characteristic width of the leg
V	characteristic volume
F_r	reaction force
v_b	takeoff velocity,
t	time
E_s	the stored energy
ε_m	mechanical efficiency
σ	surface tension
m_i	Mass of each component
a	Body length
L	Leg length
θ	Initial body angle
k	Actuator stiffness
l_i	Actuator initial length
s	Actuator stroke

T	kinetic energy,
V	potential energy,
v_i	velocity of each component,
I_i	second moment of inertia
w_i	angular velocity of each component
h_i	height from the ground level
F	actuation force
a	moment arm of the passive trigger
L_t	passive trigger length
w	width of passive trigger
t	thickness of the cantilever
δ	required deflection for passive triggering
E	characteristic modulus of the composite material
k_w	stiffness of the water surface,
d	sinking depth
C_D	drag coefficient

List of Tables

List of Figures

Contents

Chapter I. Introduction

I.1 Motivation

I.1.1 Biologically Inspired Robotics

Nature creatures sometimes show remarkable mobility that recent machines or robots cannot do. Extreme locomotion of the nature creatures inspires the robotic researchers to design the robots that are capable of overcoming and breaking limits of mobility due to its inherent morphology or environmental obstacles in various unconstraint or hazardous environment. Robotics researchers try to understand how nature creatures move and abstract design principles of robots from diverse research of biology. The principles that are carefully abstracted from bio-mechanisms of nature may give great insights for developing novel types of robots that do not exist, and enhancing performance or efficiency of various existing robots and machines in advance.

Generally, extreme movement and locomotion of nature creatures have inspired the robotic researchers in aspect of mobility and agility improvement. The humanoid is also one of representative biologically inspired robot that mimics the human [1, 2]. We expect that it works in hazardous environment as well as ordinary workplace instead of human. In addition, numerous creatures that shows remarkable movement, locomotion, and agility, have inspired the robot design. In ground robots, adaptability and stability of crawling robots could be improved by applying the principles in movement and mechanism of the cockroach [3-5]. In aerial robots, the insect scale flapping flying robot took off and flied freely in 3D space using flapping wing by mimicking flapping flying insects such as bee and flies [6, 7]. Many underwater robot is inspired by

fishes for improving efficiency and speed of swimming in water [8]. In order to achieve high mobility or to overcome the limitation of moving speed in small scale, ground robots employ the jumping locomotion and the design is inspired by the anatomy and jumping mechanics of jumping animals [9-13]. Vertical climbing on the smooth surface such as glass had been realized using the principles of the dry adhesion mechanism of the Gecko foot [14].

As described above, the robot mobility have improved thanks to the principles learned from nature creatures. In this thesis, we would add one more extreme locomotion in robotic locomotion. The teacher in nature is the water strider. The water strider have remarkable mobility on the water surface including walking, sliding, jumping on water. The robotic water strider itself can be used as pollution detector in pond or river in the future. Moreover, various technology developed for making the real insect scale robotic water strider, are expended to other industry as enabling technology that did not exist before.

I.1.2 Extreme Locomotion of the Water Strider

As described in previous section, some species of animals show extraordinary capability of movement in specific environment that is inappropriate for moving. As an example of them, water strider shows impressive locomotion on water. However, the mechanism of jumping on water is poorly understood theoretically. In this thesis, water jumping capability of the water striders is studied and the principles of the mechanism are abstracted for applying to the design of the real scale water strider robot that can jump effectively on water.

Water strider normally lives on the water surface and its main locomotion is rowing by driving legs. Sometimes, it jumps and leaps out of the surface smoothly for escaping from predators. Common water striders that we can see around pond or stream, has about 2~3cm in body length, 50 mg in body weight, and 3cm in leg length. Those are very light and small insects but they show remarkable movement on water in engineering point of view. In several researches, water strider slides and jumps in peak speed of 150 cm/s [15-18]. With this takeoff speed, the water striders can jump about 12cm high. Surprisingly, we can find there is no large splash and waves around the water strider when it jumps on water. It means that the momentum of water transferred from the driving legs of the water strider is very small. The water strider jumps on water effectively without an energy leakage to water. The criteria for effective jumping on water is addressed in this thesis.

I.2 Challenges in Developing Robotic Water Strider

I.2.1 Bio-Hydrodynamics for Jumping on the Water Surface

Mechanism of the jumping on water has been poorly understood in advance. It is hard to imagine that the robot jumps and leaps out of the water surface before seeing the behavior of the water strider. The water strider jumps and leaps out of the water surface smoothly without large splash. Thin and long legs of the water strider push down the water surface and get the reaction force from the surface. Surprisingly, the water strider floats on water effortlessly and freely moves. Moreover, when it jumps, its thin legs do not break and penetrate the water surface. There are hydrodynamic secrets behind the mechanism. We should find and verify the secrets and abstract the principles for applying to the

design of the robotic water strider.

I.2.2 Manufacturing of the '*at scale*' Robotic Water Strider

The normal water strider has dimensions of 2~3 cm in body length, 3~4cm in leg length and around 50mg in weight. It is quiet small compared to conventional robots and machines we have seen before and very light, 1/6 of a normal nut (3mm, 312 mg) which is a basic component of conventional machines. The small scale jumping robots developed in advance are still quiet big and heavy such as 7g jumping robot [10]. In order to make the real scale robotic water strider, we need to apply new manufacturing technique with novel materials. At first, we should select proper actuator that has high power density to drive the legs in small scale as describe above. In addition, materials for the body structures have to be chosen carefully for effective performance of the robot.

I.2.3 Controllable Mechanism Design in Small Scale

The robotic water strider have to be controllable by command of the external signal. Therefore, the mechanism is required to have a triggering component for active control of jump timing such as latch mechanism and it should be scalable design for miniaturization in real insect scale. Fundamentally, the mechanisms have to include the actuation part for storing energy and the triggering part for the robot to jump. As described in previous session, the mechanism should be compatible with manufacturing process and materials to be used in fabrication.

Considering these requirements, the mechanism design of the robotic water

strider is performed in integrated point of view for satisfying the jumping objectives in constraints of manufacturing, material and scale.

I.3 Objectives and Contribution

I.3.1 Research Objectives

The goal of this research is the development of the real insect scale robotic water strider that reflects principles of water jumping locomotion including the integrated design and fabrication technologies using novel manufacturing process and smart materials. As detail research objectives, three issues are studied and addressed in this thesis as follows.

First, I abstract the principles of the water jumping locomotion that is observed in movement of the water strider. The principles would guide to design the robotic water strider and the results verify the principles in nature.

Second, the manufacturing process based on smart materials that are appropriate for small scale robot are developed and evaluated. Considering the scale of the water strider, conventional machining process and normal metallic materials are hard to apply to the meso-scale (millimeter-centimeter scale) robotic systems. To deal with fabrication issues, fiber reinforced composite material based precision laser machining and laminating process would be employed and the detail design is performed in order to be compatible with the process.

Third, the robot mechanism design should be scalable for miniaturization with enough energy storage and controllable to adjust jump timing. In order to

generate enough takeoff velocity, the actuator has high power and the body structure endure high stress in meso-scale. Moreover, the energy should be released quickly by triggering like the catapult. The triggering mechanism is inserted to control the jump timing like a latch mechanism. In this thesis, the flea inspired catapult mechanism is employed to realize all these requirements.

I.3.2 Contribution

In advance, the robotics technologies have developed rapidly and broadly for improving the quality of human life and resolving an accidental problems that human cannot deal with. The development of the robotic water strider would deliver various technical improvements and knowledge about understanding the mechanisms in nature.

- The manufacturing technologies evolving from the development of the robotic water strider might expend the diversity of the scale in the robotic systems.

- The smart materials enables the system to be more efficient and it resolves the uncertainty in modeling when the unique properties of the novel materials are well evaluated and used properly in robotic systems.

- The principles in nature can be verified with artificial bio-mechanisms. Various theories and hypothesis in secrets of mechanisms in nature is hardly proved practically. In addition, practical implementation gives not only ideal outcome but also

many extra knowledge behind the principles that we should consider in real world.

Chapter II. Bio-Hydrodynamics of Water striders

The propulsion mechanism of the water striders is described with hydrodynamic forces generated by the driving legs on the water surface. To jump on water, the legs push the water surface and enough hydrodynamic forces should be generated as the reaction force for the high vertical momentum of the body. In this chapter, hydrodynamic forces around the driving legs are investigated to estimate how much the maximum reaction force the robot can obtain. Finally, the design criteria of the robotic water strider is established in order to achieve maximum efficiency on water jumping.

II.1 Previous Research

Water walking mechanisms of water striders and other water walking insects have been studied for several decades, though the jumping mechanisms have been less investigated [16, 17, 19-22]. As described in Newton's second and third laws, the water walking creatures gain the momentum by pushing the water surface with driving legs and the magnitude of reaction force from water determines how fast they can move. Early researches assumed that capillary waves of the water surface are the dominant means of momentum transfer. However, Denny M. W *et al.* [15] showed that some small infant water striders could not produce enough velocity to make capillary waves, which called Denny's paradox. Hu D. L. *et al.* [17] discovered and explained that the more

exact means for the momentum transfer of small water striders was hemispherical vortices shed produced by its driving legs. Therefore, we have understood that almost small water walking creatures can move forward on the water surface by the momentum transfer through capillary waves and vortices shed.

On the other hand, water jumping mechanisms have been less understood. Unlike the walking which is the lateral motion, the jumping requires the high enough momentum in vertical direction. Water striders shows the elegant jumping motion, leaping out of the water surface smoothly, when it escapes from predators. Very thin (<100 μm) wire shaped driving legs push down the water surface and the surface endures the driving force of legs when the legs does not penetrate the water surface. The applied force and velocity is observed approximately 80 mN/m and 100 cm/s which values are not exceed maximum surface tension, 150 mN/m [17]. These values from the motion of water striders are important criteria for developing and designing the robotic water strider. In aspect of hydrodynamic condition for water jumping, Lee et al. [23] investigated behavior of hydrophobic solids interacting with free surface of water by finding condition for sinking, bouncing and oscillation depending on density and velocity of the free-fall solid sphere. The results give insight to understand characteristics of the water surface when it is exerted by impulse of the objects.

Hydrophobicity is the one of crucial properties for floating and moving on the water surface. Water striders have remarkable non-wetting legs which have super hydrophobic hierarchical hairy structures [19]. The super hydrophobic

legs enables the water striders to stand effortlessly and move rapidly on the water surface using the surface tension force. Generally, higher hydrophobicity of the legs induces larger maximum surface curvature force by the surface tension of the water and deeper sinking depth without breaking the surface.

Based on these previous research, the hydrodynamic forces for jumping on the water surface can be categorized and analyzed to understand the mechanism of jumping on water. The reaction force between the driving legs and the water surface is determined by the driving force as described in Newton's second law. By the reaction force, the robot obtains the vertical momentum to take off. Therefore, the hydrodynamic forces generated by the water surface are the most importance constraints for designing the power of the actuators. In following sections, the principles of jumping on water are addressed in aspect of the hydrodynamics and the design criteria is derived.

II.2 Hydrodynamic Forces on the Water Surface

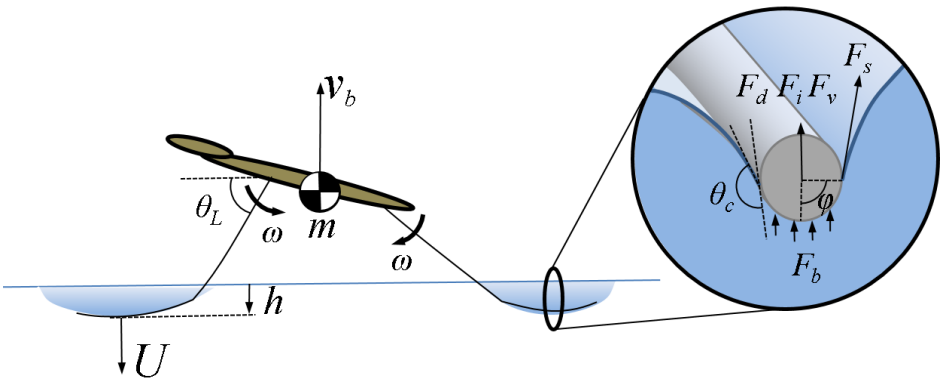

Figure II. 1 Illustration of hydrodynamic forces exerted to the leg of the water striders on the water surface

The lifting force in jumping on water is created from various hydrodynamic forces between driving legs and water surface while the reaction force on the rigid ground directly lifts the body in case of jumping on the ground. Figure II. **1** shows the dynamics of the water-strider and the hydrodynamic forces between the leg and the water surface. The form drag force, F_d, and the viscosity force, F_v, are created by hydraulic pressure of water to the moving leg with certain velocity. The buoyancy, F_b, and the surface tension, F_s, are the forces that are exerted to the submerged objects. The added inertia, F_i, arises when the fluid is accelerated by the accelerating leg. Finally, Marangoni force, F_m, is generated in the gradient of surface tension. Each terms are expressed as follows [18],

$$\left|F_r\right| \sim \rho U^2 A + \rho g h A + \rho V \frac{dU}{dt} + \mu U A + \sigma \frac{1}{w} A + \nabla \sigma A \qquad (1)$$

Form Drag	Buoyancy	Added mass	Viscosity	Curvature	Marangoni
F_d	F_b	F_i	F_v	F_s	F_m

where ρ is density of water, U is speed of the leg, A is the characteristic area of the leg, μ is the viscosity of water, g is the gravitational acceleration, h is the depth of the leg from the free surface of water, γ is the surface tension coefficient, w is the characteristic width of the leg, V is the characteristic volume. Marangoni force term can be eliminated since gradient of the surface tension is zero.

II.3 Energy and Momentum Transfer for Jumping

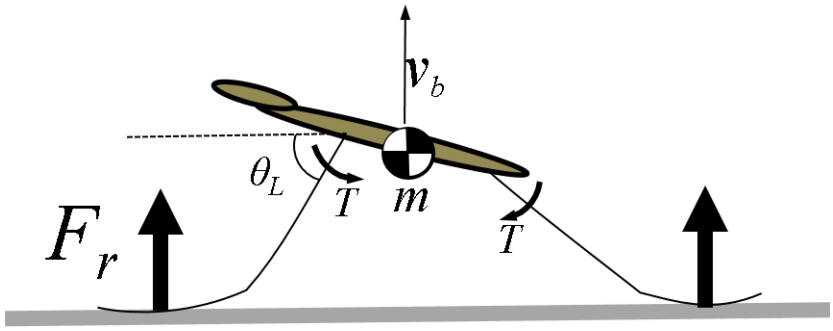

Figure II. 2 Free body diagram of the water strider jumping on ground

The jumping creatures jump by momentum with reaction force from the jumping surface. The stored energy in the body is transferred to the vertical kinetic energy and other losses such as vibration, friction *etc.*.

II.3.1 Jumping on the Rigid Ground Surface

Before considering jumping on water, the principals of jumping on ground would be basic knowledge we have to understand. The jumping creatures have driving legs to push ground. As described in Newton's second law, the legs have the reaction force from the ground surface. The reaction force, F_r, from the ground surface accelerate the body to have enough take off velocity. The velocity is determined by the reaction force subtracting the body weight and exerted time as following the momentum equation,

$$mv_b = \int (F_r - mg)dt \tag{2}$$

where m is the body mass, v_b is the takeoff velocity, g is the gravitational acceleration, t is time. In aspect of the energy transfer, the stored energy, E_s, in the body is transferred to the vertical kinetic energy, $mv_b^2/2$, and the vibration of the legs and the body, the friction loss as follows.

$$E_s \rightarrow \frac{1}{2} m v_b^{\,2} + vibration + friction\,loss + \ldots \tag{3}$$

The ratio of the vertical kinetic energy to the stored energy is defined as the mechanical efficiency (ε_m), which is the inherent property of the jumping mechanism.

$$\varepsilon_m = \frac{1}{2} m v_b^{\,2} / E_s \tag{4}$$

The takeoff velocity can be calculated by the energy equation with the stored energy and the mechanical efficiency as follows,

$$v_b = \sqrt{\varepsilon_m 2E_s / m} \tag{5}$$

In this research, the energy source is the thermal elastic actuator, the shape memory alloy coil actuator. Therefore, the stored energy can be expressed as the elastic potential energy,

$$E_s = \frac{1}{2} k s^2 \tag{6}$$

where k is stiffness of the actuator, s is the actuation stroke. Finally, the takeoff velocity equation by energy transfer is expressed as follows,

$$v_b = \sqrt{\varepsilon_m k s^2 / m} \tag{7}$$

If the actuation stoke is fixed, the stiffness of the actuator have linear relationship with actuation force, and the reaction force is linear to the actuation

force too. Therefore, the reaction force can be design by the stiffness of the actuator. On the ground, the reaction force is unlimited as much as the actuation force. We can increase the takeoff velocity by increasing stiffness of the actuators as much as the force that the body structure can endure.

II.3.2 Jumping on the Water Surface

On the water surface, the reaction force is generated by the hydrodynamic forces exerted on the driving legs when the legs push down the water surface. The hydrodynamic forces described in the previous session are determined by the driving force and the velocity of the driving legs. The hydrodynamic forces on the water surfaces are totally different according to whether the legs break the water surface or not, because the surface curvature force which is the largest force among the hydrodynamic forces is lost when the surface is broken. Using characteristic values of the water strider's parameters, approximately the magnitudes of each term in hydrodynamic equation (1) are estimated. The characteristic properties of the water striders are listed in Table II. 1 adopted from D. L.Hu *et al.* [17].

Table II. 1 Characteristic Parameter Values of the water strider

Parameter	Description	Characteristic Value
ρ	Density of water	10^3 kg/m^3
U	sinking velocity of the leg	0.4 m/s
l_s	Submerged length of legs	10 mm
w	Diameter of legs	0.1 mm
A	Submerged characteristic area (l_s x w)	10^{-6} m^2
g	Gravitational acceleration	9.8 m/s^2
h	Submerged depth	4 mm
V	submerged characteristic volume	4x10^{-9} m^3
μ	Viscosity coefficient of water	10^{-3} N•s/m^2
σ	Surface tension of water	0.072 N/m

Approximated magnitudes of terms in equation (1) are calculated as Table II. 2. The surface curvature force which is exerted by the surface tension of the water surface is much larger than other force in a factor of 4.5. We think that the thin wire shaped legs have very small characteristic area and volume, and minimize the form drag, buoyancy and added mass effect. Basically, viscosity of water is small, and the viscosity force is small with this velocity. Therefore, the dominant force that can be the reaction force of the water strider is the surface curvature force. However, the surface curvature force exists unless the water surface is not broken. If the legs penetrate the water surface, the surface curvature force disappeared immediately.

Table II. 2 Approximated hydrodynamic forces exerted on the driving legs

Term	Description	Approximated Force
$\rho U^2 A$	Form drag	160 μN
$\rho g h A$	Buoyancy	4 μN
$\rho V \frac{dU}{dt}$	Added mass	160 μN
$\mu U \frac{1}{w} A$	Viscosity	4 μN
$\sigma \frac{1}{w} A$	Surface curvature	720 μN

Figure II. 3 shows the maximum hydrodynamic forces in two cases of non-breaking and breaking the water surface. When the water surface is broken, the maximum hydrodynamic force decrease dramatically because the surface curvature force that is the largest force is disappeared.

A sudden drop of the reaction force causes the drastic decrease of the takeoff velocity according to the equation (2). In aspect of the energy transfer,

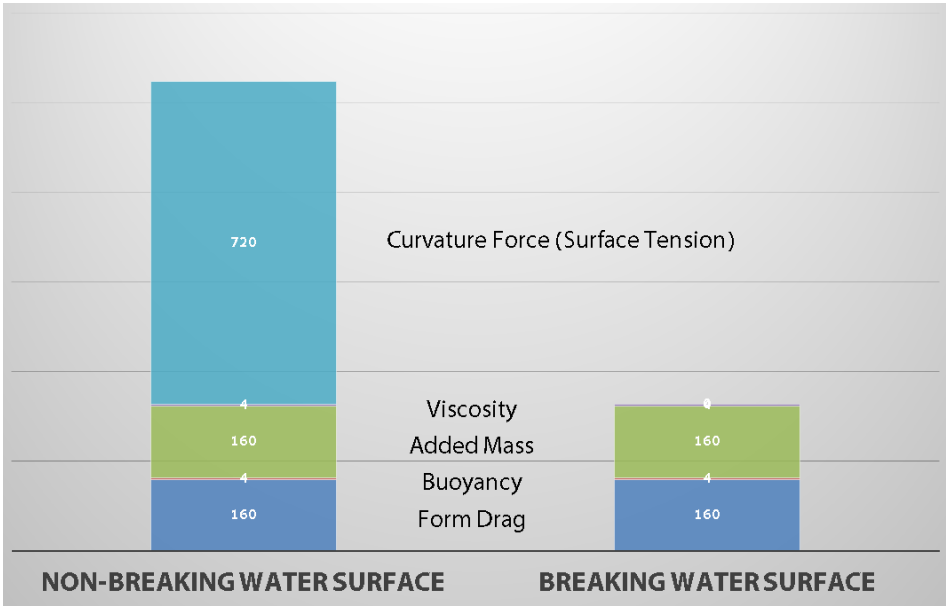

Figure II. 3 Comparison of the hydrodynamic forces when the water surface is broken and unbroken

the momentum of water around the legs increases when the legs break the water surface, and the energy loss to the kinetic energy of water causes reducing the vertical kinetic energy of the water strider as following energy flow.

$$E_s \rightarrow \frac{1}{2} m v_b^{\,2} + water\ kinetic\ E + vibration + friction\ loss + \ldots \quad (8)$$

Therefore, the water strider cannot achieve the velocity as jumping on the ground expressed as equation (7).

II.4 Design Criteria of the Robotic Water Strider

The surface curvature force is dominant reaction force that can be generated on the water surface by thin wire shaped legs. Therefore, the robotic water strider should not break the water surface for effective jumping on water. With this principal, we define the design criteria of the robotic water strider as non-breaking the water surface. To satisfying the criteria, the reaction force per unit submerged perimeter should be below the maximum surface tension (σ).

$$\frac{|F_r|}{Surbmerged\ Length} \leq 2\sigma \quad (9)$$

In case of jumping on water, the typical value of the surface tension (σ) is *0.072 N/m*. Consequently, the robotic water strider should be designed to have the maximum reaction force per unit submerged length below the maximum

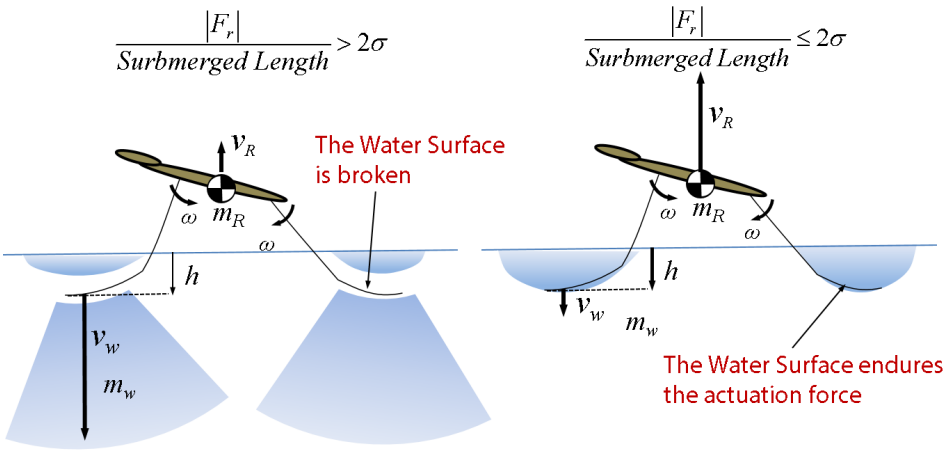

(a) (b)

Figure II. 4 Illustration for comparing the robot behavior when the water surface is broken, (a), and unbroken (b)

surface tension (2σ).

If the driving legs break the water surface, the legs sink rapidly under water and the robot cannot obtain enough momentum for takeoff as shown in Figure II. 4 (a). In contrast, when the water surface is not broken, the curvature force endures the driving force and the robot obtains the maximum momentum like jumping on ground as shown in Figure II. 4 (b).

Chapter III. Design and Fabrication

The mechanism for satisfying the design criteria described in previous section is designed by employing the flea inspired catapult mechanism [12, 13, 24]. According to the design criteria, the robot should not exceed the reaction force over the maximum curvature force to have large hydrodynamic force. In addition, the robotic water strider have to obtain enough momentum for takeoff. In these constraints, the optimal reaction force profile can be derived for the maximum momentum with the lowest reaction force. To obtain the optimal reaction force profile, the actuation time should be expanded for increasing the momentum of the robot with the lower force.

The simplest jumping mechanism can be made by using the spring like legs. Compressed legs are released rapidly by triggering. They push down the ground and the body is accelerated by the reaction force. The vertical momentum of the robot is determined by integration of the reaction force through the exerting time. Inherently, simple elastic legs have the maximum force at the beginning of the actuation as shown in Figure III. 1 (a), and the reaction force decreases gradually. In that case, the momentum transfer is limited by the maximum reaction force. It is hard to increase the momentum maintaining the low reaction force. However, there is a catapult mechanism that has unique force profile during actuation. The flea inspired torque reversal catapult mechanism shows different force profile when the stored energy is released. The reaction force of the torque reversal catapult mechanism increases gradually from the beginning of the actuation and has the maximum force during the actuation as shown in Figure

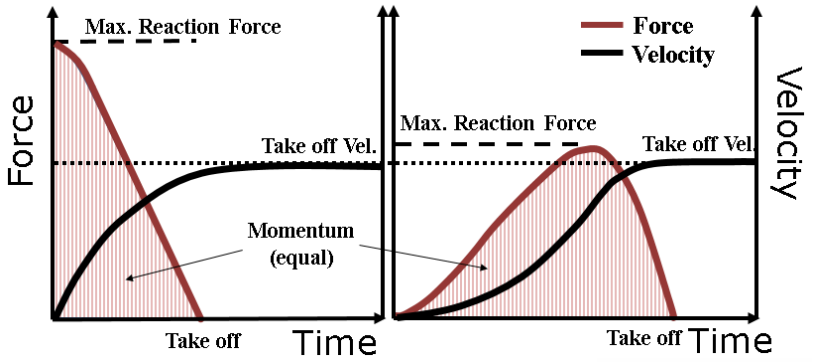

Figure III. 1 Reaction force profile (a) elastic legs model (b) desired force profile (Flea's torque reversal mechanism)

III. 1 (b) [12, 25]. The actuation force is distributed along the actuation time and it enables to increase the momentum transfer with maintaining the low reaction force. The detail description of the mechanism follows at next section.

III.1 Flea Inspired Catapult Mechanism

III.1.1 Flea's Torque Reversal Catapult Mechanism

A tiny insect flea, below 1mm in body length, can jumps 200 times its body length. The unique mechanism of the jumping legs enable to gradually stores elastic energy and releases it quickly. Many biologists try to understand how it can jump high with tiny body and legs [25-31]. The anatomy of the jumping legs of the flea gives a key to understand how it works [26-28, 30, 31]. The flea's jumping leg consists of cuticles, an extensor muscle, a flexure muscle, trigger muscle, and elastic materials, as shown in Figure III. 2 [12]. The flea jumps using a combination of these elements. First, the flexor fold the leg (Figure III. 2 (a)) and get ready for jumping. Next, the extensor muscle pulls the legs in the folding direction and stores the elastic energy in the muscle and resilin (Figure

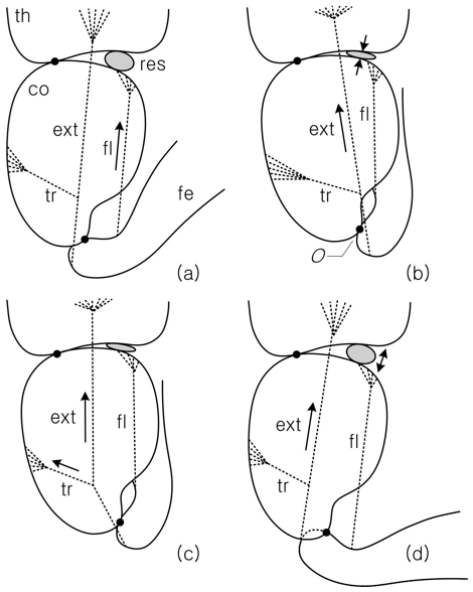

Figure III. 2 Jumping procedure of the flea's jumping legs with anatomy of the muscles and skeleton structures. It is composed of three exoskeletal links: *th* is the thorax, *co* is the coxa, and *fe* is the femur. The joint connecting the coxa and the femur is the reversal joint. A resilin pad (*res*) functions as the compression spring. Three muscles are arranged in the leg: *fl* is the flexor, *ext* is the extensor, and *tr* is the trigger muscle

III. 2 (b)). The driving leg is blocked by the cuticle body structures. After that, the small trigger muscle pulls the extensor muscle in the opposite direction and changes the torque direction respect to the rotation joint of the femur (Figure III. 2 (c)). The stored elastic energy is released rapidly when the extensor muscle passes through the joint (Figure III. 2 (d)). We call this mechanism as the torque reversal catapult mechanism of the flea.

To apply the flea's jumping principle to the jumping robot design, the flea's catapult mechanism was simplified as shown in Figure III. 3. The mechanism consists of the leg linkage, the extensor, trigger, and stopper. This mechanism produces a single catapult motion because it does not have the flexor. The components which are essential for jumping are retained in the simplified diagram.

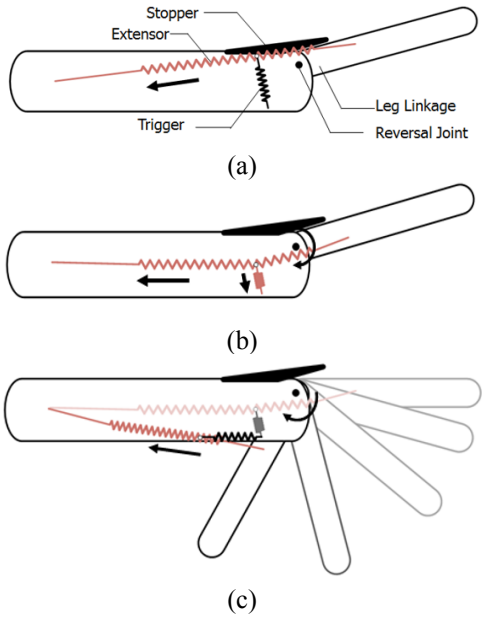

Figure III. 3 Schematic diagram of torque reversal mechanisms inspired by the flea's jumping leg. (a) storing energy in latched position, (b) triggering, and (c) discharging elastic energy

The extensor pulls the leg linkage blocked by the stopper and stores the elastic energy by increasing the stiffness (Figure III. 3 (a)). The trigger pulls the extensor slightly to change the direction of the torque (Figure III. 3 (b)). For changing the torque direction, the reversal joint should be designed such that the extensor can pass through the joint. Immediately after the extensor passes through the reversal joint, it pulls the leg and produces rapid rotation (Figure III. 3 (c)). In the presence of a flexor, it can repeat this motion.

With this mechanism, Noh *et al.*[12] and Koh *et al.* [13] developed light jumping robots with a similar configuration to that of the flea's leg. The jumping mechanism design was simplified by retaining only the parts required for jumping. Figure III. 4 shows a comparison of the existing and proposed mechanism designs. (a), (b) are the schematic deign of the first [12] and second version [13] of the flea inspired jumping robot and (c), (d) are prototype of the

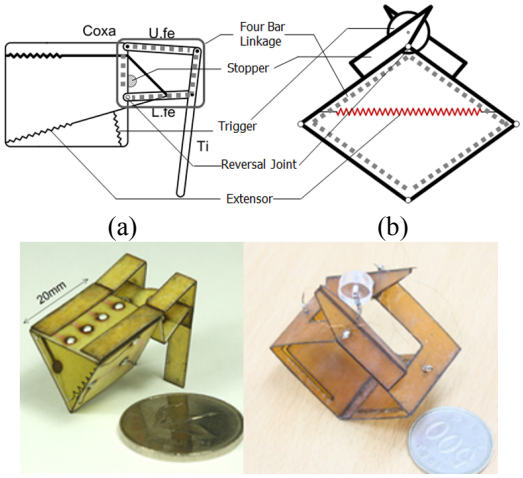

Figure III. 4 Previous design of two flea-inspired jumping mechanisms

each design. The main difference between the two mechanisms is that the second version (b), (d) does not have the coxa that is the body for attaching the actuators. The second version has only the four-bar linkage body, indicated by the gray dotted lines, whereas the previous design has the coxa and the tibia attached to the four-bar linkage. In addition, the second design separates the trigger and the extensor. The trigger pushes the extensor in the opposite direction with a pusher attached atop the four-bar linkage, as shown in Figure III. 4 (b).

The previous flea inspired jumping robots have glass fiber reinforce composite body structures with the embedded circuit and the SMA coil spring actuators as an artificial muscle. The first version jumps 64 cm and the second version jumps 120 cm [12, 13]. The specifications of the robots are listed in Table III. 1.

Table III. 1 Specification of flea inspired jumping robots.

	1st Version	2nd Version
Robot Specifications		
Weight	1.1 g	1.11 g
Size	20 mm	20 mm
Jumping Height	64 cm	120 cm
SMA Coil Spring Actuators		
Wire Dia. (d)	254 μm	254 μm
Coil Dia. (D)	1 mm	1.25 mm
Spring Index (D/d)	5.4	5
Coil Number (n)	11	19
Spring Const.(k) (actuation)	600 N/m	240.2 N/m
Actuation Length	7.15 mm	16.6 mm

The flea inspired jumping robots can jump much higher by storing more elastic energy in actuators with higher stiffness and larger actuation stroke. The jumping time is controlled by triggering actuator witch induce the torque reversal.

III.2 Conceptual Design and Fabrication

Previously, two types of jumping mechanisms have been developed based on the torque reversal principal inspired by fleas as shown in Figure III. 4. The first prototype was 2 cm long, weighed 1.104 g, and jumped 64 cm [12]. The second prototype had a simplified design and low-profile jumping shape with a height of about 10 mm and jumping distance of 1.2 m [13]. The unique jumping mechanism of the flea's leg inspired the development of these meso-scale robotic jumping insects. The basis of these robots is a torque reversal mechanism – a catapult mechanism – that rapidly transfers stored elastic energy into kinetic energy. With a muscle or a smart actuator that can change its

stiffness, it is categorized as an active storage and active release catapult mechanism in Table III. 2. The torque reversal mechanism is composed of three main components; an extensor muscle, a stopper, and a triggering muscle.

Table III. 2 Catagorization of Various Catapult Mechanisms for Jumping

Symbol	Passive Storage	Active Storage
Passive Release	Grillo [32] 7g robot [10] Closed elastic [33] Jollbot [34] Mini-Whegs [9] L. Xiao *et al.* [35]	**Design in this paper**
Active Release	Circular robot [36] Jumping microrobot [37] Hooper [11]	FLEA v1[12], v2 [13]

Compared to other catapult mechanisms, which commonly have latches (e.g. small pin-like elements or friction detents) the torque reversal mechanism presented in this thesis utilizes a bistable structure to store and rapidly release elastic energy. This is an advantage for miniaturization since such a mechanism doesn't need small mechanical elements for a latch or precision friction, both of which are hard to repeatable produce on the millimeter scale. The previous two robot mechanisms demonstrated the feasibility of developing a small scale jumping robot with the torque reversal mechanism inspired by the flea's jumping leg.

The Smart Composite Microstrucures (SCM) process is applied to produce the millimeter- scale flexure-based linkages of the jumping mechanism [38]. This process creates laminated composites of bulk-machined materials that form structures and mechanisms based on folded flexure joints with feature sizes ranging from micrometer to centimeter. The quality of the SCM is improved by

using cured carbon composites and adhesive layers in the process. It reduces problems caused by misalignment of prepregs during layering and the overflow of the resin during the curing process. Furthermore, folding is automated by using pop-up book MEMS techniques [39].

III.2.1 Mechanism Design of the Robotic Water Strider

A smaller and lighter torque reversal mechanism design is introduced and the design is compatible for applying the SCM and pop-up book MEMS processes. The current design has simple structure by removing the triggering actuator from the previous design [12, 13]. It is replaced by a passive triggering mechanism which is described in detail in the following section. A thin, laser-cut sheet SMA actuator is employed as the extensor actuator. It is a suitable actuator for millimeter-scale robots and compatible with the SCM and pop-up book MEMS processes considering its high energy density and thin profile.

It is simplified to contain only three essential components, each compatible with the SCM and pop-up book MEMS manufacturing and assembly processes. The manufacturing process is described in detail in the following fabrication section. Compared to jumping mechanisms in Figure III. 4, it is clear that the

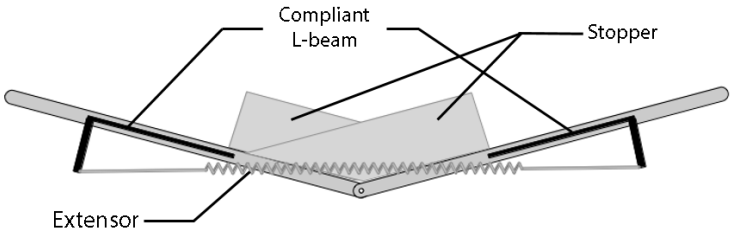

Figure III. 5 Schematic design of the torque reversal catapult mechanism for the robotic water strider

mechanisms become simpler and more compact through the removal of redundant elements. In the second prototype (Figure III. 4 (b), (d)) the Coxa structures and the long legs are removed from the first design (Figure III. 4 (a), (c)). The current design replaces the triggering actuator with a compliant L-beam component. The effort involved in this laborious assembly process can be reduced by design simplification. As the L-beam bends, the actuator passes through the center of the rotation; this causes the torque to reverse its direction and allows the robot to open its legs for jumping. This L-beam incorporates the storage and triggering components to reduce the number of actuators for the entire system. The linkage structure with a stopper is similar to the second design, and the stoppers block the two links bending upward, as shown by the shape in Figure III. 5. The extensor is an artificial muscle actuator with variable stiffness characteristics. SMA is a suitable artificial muscle actuator for the torque reversal mechanism with its unique variable stiffness property depending on temperature. Table III. 2 categorizes the catapult mechanisms; the third type can be considered to be an active storage and passive release catapult mechanism. The elastic energy is stored in the extensor and the L-beam as the stiffness of the extensor is increased and automatically released when the critical bending of the compliant L-beam is exceeded.

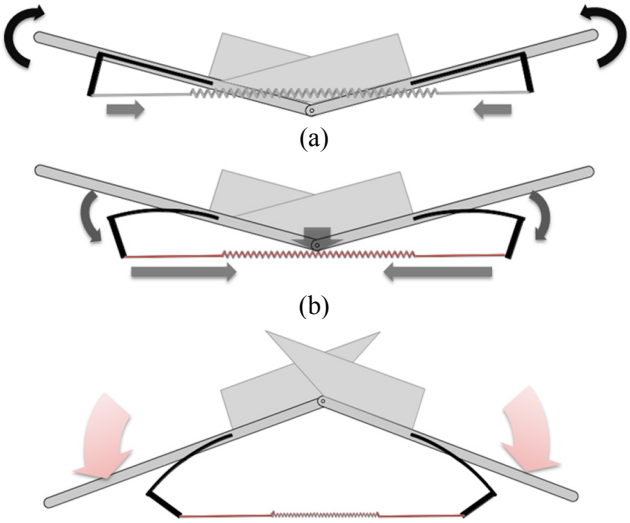

Figure III. 6 The jumping procedure of the passive torque reversal catapult mechanism of the robotic water strider

The jumping process of the current design has three steps, as shown in Figure III. 6. At the initial position, shown in Figure III. 6 (a), the extensor has a low stiffness, and the small torque is exerted upward with respect to the rotation joint at the center of the structure. The stoppers block the links and maintain the initial position. When the extensor increases the stiffness and the pulling force exerted at the arm of the compliant L-beam, the L-beam starts to bend, and the extensor moves down as shown in Figure III. 6 (b). At this step, the elastic energy is stored in the extensor and compliant L-beam. Immediately after the extensor passes through the rotation joint, the direction of torque exerted on the structures is reversed. The reversed torque rotates the links downward, and the stored elastic energy explodes to rapidly transform into kinetic energy, as shown in Figure III. 6 (c). As the links rotate, the moment arm—which is the normal distance between the extensor and rotation joint—

increases, and the torque increases rapidly. With this mechanism, the two links work as the jumping legs. To magnify the rotation radius of the links, we placed longer wire legs in the final prototype.

III.2.2 Fabrication Process

The robot structure was designed so that the SCM manufacturing process could be applied; this process is described in the following section. This process facilitates the development of microscale linkage structures by lamination of multiple sheets cut by precision laser machining [38]. In this manufacturing process, the planar folding pattern is folded into 3D shapes to become the final robot structure after adhesion. Therefore, a 2D folding pattern design is needed for the robot structures, unlike traditional mechanical design.

The upper figure in Figure III. 7 is the 2D folding pattern design of the current jumping mechanism. The solid line is the cutting line for laser machining. The tooth shape cutting lines are folding joints connected by a flexible polymer

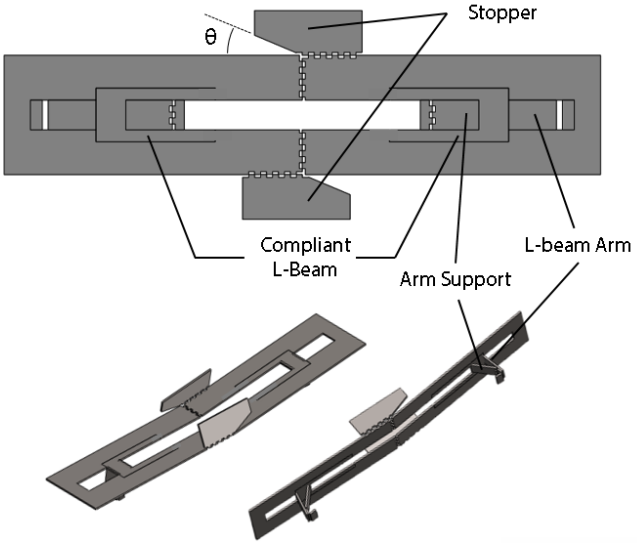

Figure III. 7 Planar design (upper) and folded shape (low) of body structure

film. This line shape shortens the length of the exposed flexible film and prevents buckling [40].

Angle θ of the stopper determines the initial shape of the jumping mechanism when ready for jumping, as shown in Figure III. 6 (a). The length of the L-beam arm and angle θ are the important design parameters for positioning the extensor. The extensor should be located between the L-beam virtual bending joint and rotation joint of the links because the L-beam must be bent downward to reverse the torque direction. In this prototype, θ was set to 32°, and the length of the L-beam arm was set at 1.7 mm based on the computed kinematic relationship. The arm support is to distribute the stress concentration at the L-beam folding joint.

The lower part of Figure III. 7 shows the folded structure from the 2D pattern design. The only active joint is the rotation joint at the middle of the structure connecting two links. The extensor is at the tip of the L-beam, which has small links for attaching the extensor.

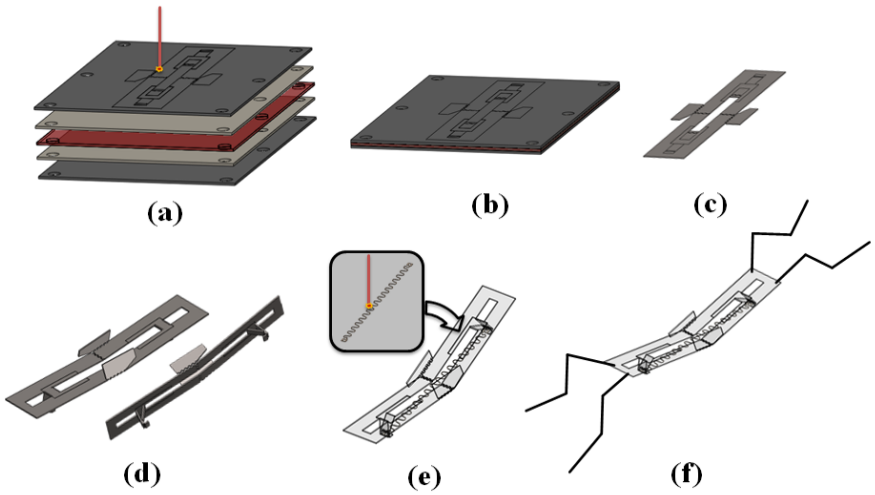

Figure III. 8 Manufacturing process of robot structures

As noted in the previous section, the robotic jumping insect was fabricated using the SCM process, which involves laminating multiple layers of materials. Figure III. 8 shows the fabrication procedure. Five layers are needed for the linkage structure: two fiber reinforced composite plates, two adhesive layers (FR1500, Dupont Co.), and a single polyimide film layer (Kapton, Dupont Co.). Each layer is precisely cut by a UV laser (355 μm wavelength), as shown in Figure III. 8 (a). Each layer has an alignment pin hole and is laminated in the order of composite plate → adhesive → Kapton → adhesive → composite plate. After alignment, the structure is pressed with heating at about 80 psi and 250 °C for 3 h, as shown in Figure III. 8 (b). This is the curing step. A laser is used to cut the outline of the layout for the final cut; the folding pattern of the robot linkage is shown in Figure III. 8 (c). The folding structure is folded and fixed by epoxy adhesives, as shown in Figure III. 8 (d). An extensor, which is the actuator of the robot mechanism, is placed on this linkage structure.

The extensor is made from a sheet of SMA. SMA is a suitable material for

the extensor; it is an artificial muscle actuator with unique variable stiffness characteristics. Furthermore, using a sheet for the actuator shape is compatible with the lamination manufacturing process. The SMA has an actuation strain range of about 8%–10%. To magnify the actuation stroke, we cut the sheet SMA into a wrinkled shape, as shown in Figure III. 8 (e), with a UV laser. With this pattern, the sheet SMA actuator creates an actuation strain range of above 100%. Each end of the sheet SMA actuator has a small hole to increase the adhesion surface with the robot structure. Figure III. 9 shows the sheet SMA coil actuators cut by the UV laser machine.

The wrinkled sheet SMA actuator is attached at both ends of the L-beam arm with the shape polymer riveting [41], and epoxy adhesives as shown in Figure III. 8 (e). Finally, four legs are used to magnify the rotation radius when the robot jumps as shown in Figure III. 8 (f). The legs are made of the metallic wire. The NiCr wire was used as legs at first. However it was easily bent, so it is replaced by the superelastic shape memory alloy wire at later prototypes. Figure III. 10 is the initial prototype that uses carbon fiber composites as the body structures and the NiCr wire as the legs.

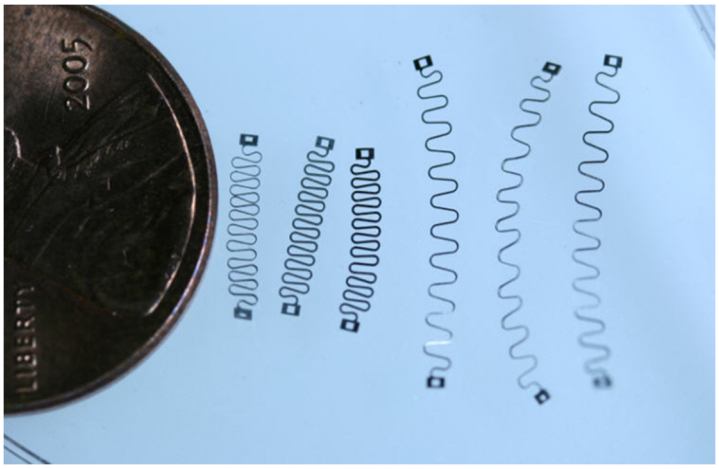

Figure III. 9 Sheet SMA coil actuators

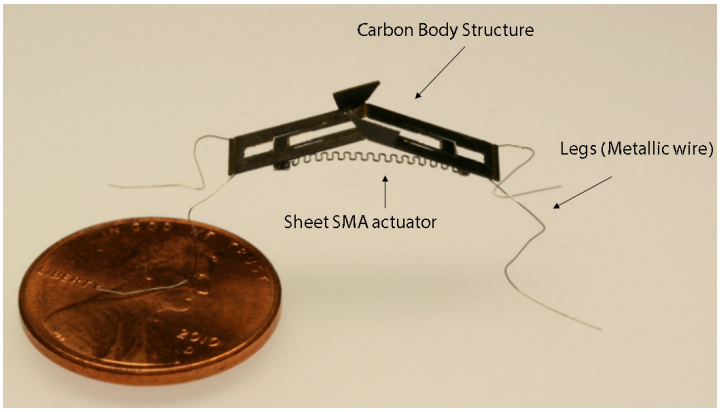

Figure III. 10 The initial prototype of the robotic water strider

III.2.3 Jumping Test on the Ground

The torque reversal mechanism was triggered a few seconds after the robot was placed on the heat plate. It took 6 ms to release the elastic energy and take off, as shown in Figure III. 11 (a). This figure shows that the compliant L-beam was bent by the extensor actuator. The four relatively long leg wires pushed the robot up, and the bending shape of the legs was beneficial for maintaining contact with the ground until takeoff.

The velocity profile during takeoff was plotted as shown in Figure III. 11 (b) using a vision analysis program (Proanalyst). The velocity of the center of mass was the actual robot velocity. However, it was difficult to determine the exact center of mass in the video. Therefore, we measured the velocity of the rotation joint and plotted it in the graph. The oscillation of the velocity profile is shown in the graph because the entire robot mechanism with legs was

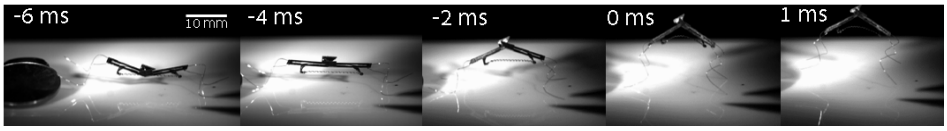

(a)

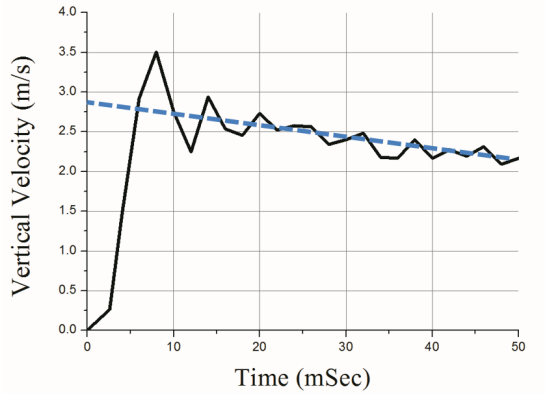

(b)

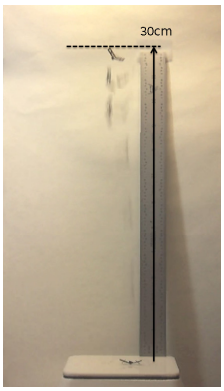

(c)

Figure III. 11 Test experiment of Flea inspired catapult mechanism

vibrating right after takeoff. This vibration caused oscillation of the velocity profile because the rotation joint was not the center of mass. The maximum takeoff velocity was about 3.5 m/s, as shown in Figure III. 11 (b). However, this cannot be considered as the takeoff velocity of the robot because the velocity of the rotation joint was much higher than that of the center of mass owing to the vibration. We assumed the takeoff velocity to be about 2.7 m/s based on the trend of the average oscillation curve. The results of several jumping tests produced a maximum jumping height of 30 cm, as shown in Figure III. 11 (c). This is about 150 times the robot body height.

III.2.4 Design and Hydrophobic Coating of Jumping Legs

Jumping legs are designed to have minimum uncertainty during takeoff. The robot swing the legs which are attached symmetrically at both end of the body. The angle between legs and the base surface change continuously during takeoff. To maintain the uniform contact condition of legs and the base surface, the tip of the leg, regarding as foot, is bent smoothly for shaping circular. The

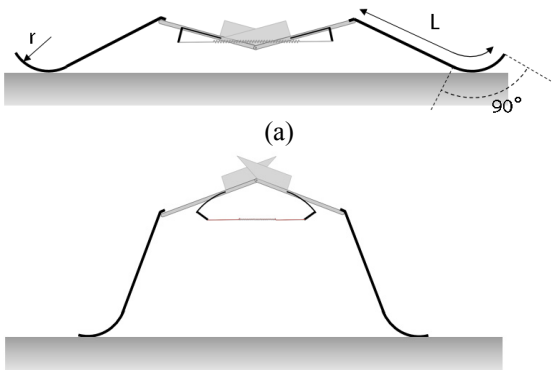

Figure III. 12 Design of Jumping Legs

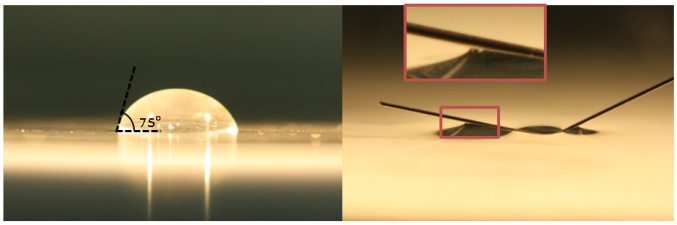

(a)

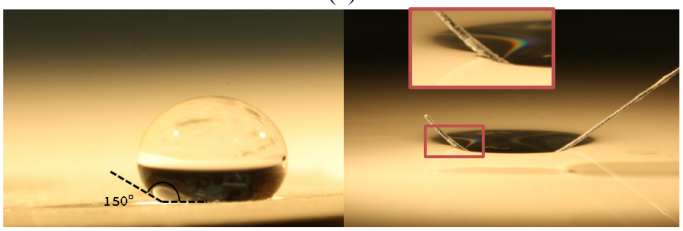

(b)

Figure III. 13 (a)Non-coated SMA (Nitinol) (b) SMA(Nininol) coated by the hydrophobic material (EverDry^{TM}, UltraTech International Inc.)

round shaped foot always contact with the base surface in tangential direction. The uniform contact condition would be applied to the robot on the water surface similarly.

Hydrophobicity enhances the maximum surface curvature force and reduces the drag force when the legs escape from the water surface. The water striders have hierarchical micro structure in the driving legs that maximizes hydrophobicity [19, 20]. There are many method for increasing hydrophobicity which is revealed by high contact angle at tri-contact point of air, water and solid. A common method is the coating with various materials that have high contact angle property [23]. The micro structures such as micro porous structures [42] using a chemical process. Recently, a commercial super hydrophobic coating product is available, called EverDry^{TM} (UltraTech International Inc.) [43]. The contact angle of the legs with water increases over 150° as shown in Figure III. 13. In a fine coating condition, the company says that the contact angle of over 170° can be achieved.

III.2.5 Design Parameters of the Robotic Water Strider

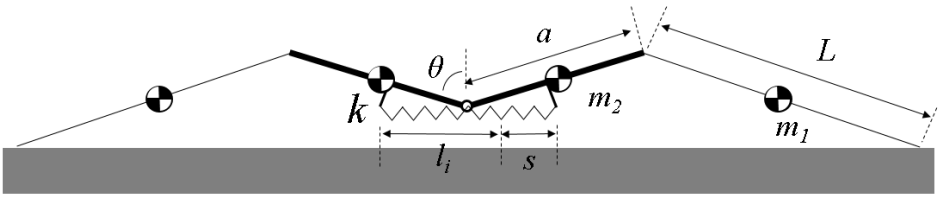

Figure III. 14 Design parameters of the robotic water strider

To design the robotic water strider for achieving the desired reaction force and jumping performance, five design parameters are selected. Figure III. 14 shows specification of dimensions and properties of the robot design. The parameters are listed in Table III. 3. The actuator stiffness and the leg length are dominant design parameters in the following modeling and experiment section for satisfying the reaction force requirement.

Table III. 3 Design Parameters of the Robotic Water Strider

Parameters	Description	Variable
m_i	Mass of each component	Dependent
a	Body length	Fixed
L	Leg length	Independent Design Parameter
θ	Initial body angle	Fixed
k	Actuator stiffness	Independent Design Parameter
l_i	Actuator initial length	Independent Design Parameter
s	Actuator stroke	Independent Design Parameter

Chapter IV. Dynamic Modeling and Experimental Results

The dynamic model of the robotic water strider at the moment of takeoff on the ground and the water surfaces is derived by solving Lagrange differential equation. Jumping experiments with various design parameters verify the model. Finally, the modeling and experimental results validate the water jumping criteria.

IV.1 Dynamic Modeling

IV.1.1 Dynamic Modeling of Jumping on the Ground

Lagrange's differential equation is derived with kinetic and potential energy equation of the robotic water strider based on the specification in Figure III. 14 as follows.

$$\frac{d}{dt}\left(\frac{\partial L}{\partial \dot{\theta}}\right)-\frac{\partial L}{\partial \theta}=0 \tag{10}$$

where $L = T - V$,

$$T = \sum \frac{1}{2} m_i v_i^2 + \sum \frac{1}{2} I_i w_i^2,$$

$$V = \frac{1}{2} k s^2 + \sum \frac{1}{2} m_i g h_i$$

T is kinetic energy, V is potential energy, v_i is velocity of each component, I_i is the second moment of inertia, w_i is angular velocity of each component, g

is gravitational acceleration, h_i is the height from the ground level. By solving the differential equation(10), we can get the equation of motion which shows position, velocity and acceleration of the robot.

The stiffness of the SMA actuator, k, is increased by increasing the temperature of the actuator. However, it is hard to measure and control the temperature precisely. In order to get the reliable stiffness of the actuator, it is calculated using the modeling of the passive trigger component and the stroke of the actuator. The beam deflection model is employed to obtain the triggering force and the stroke of the sheet SMA coil actuator can be measured. The force and the deflection of the passive trigger is expressed as equation (11), the cantilever deflection model with the width and the thickness of the passive trigger as shown in Figure IV. 1.

$$F \cdot a = 2 \cdot \frac{2EI}{L_t^2} \delta \quad (I = \frac{wt^3}{12}) \tag{11}$$

where F is the actuation force, a is moment arm of the passive trigger, L_t is length, w is width, t is thickness of the cantilever, δ is the required deflection for passive triggering, E is the characteristic modulus of the composite material.

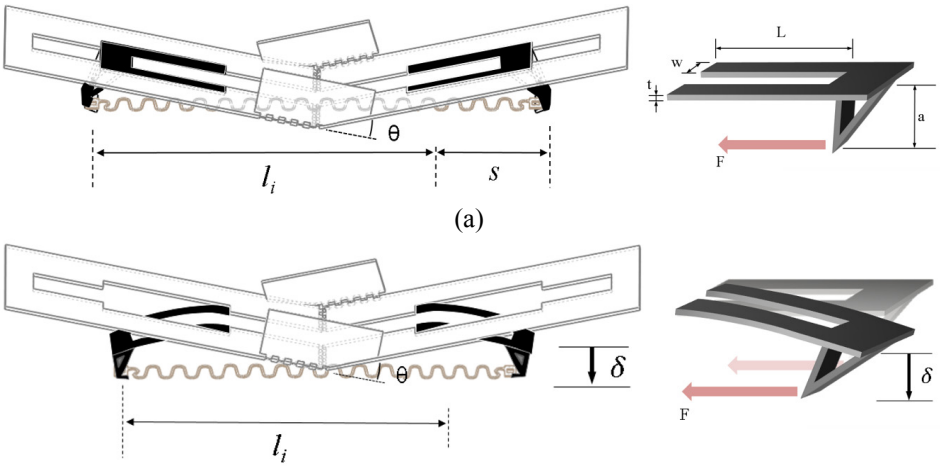

Figure IV. 1 Illustration of the passive trigger component for describing the modeling parameters. (a) Before actuation, (b) the moment of triggering.

To design the triggering force of the passive trigger by the model, the characteristic modulus of the composite material should be obtained by experiments. The experiments are performed using the tensile test machine and the vision analysis as shown in Figure IV. 2 (a). The specimen have various width and thickness of the passive trigger varying the stiffness. The pulling bar instead of the actuator pull the passive trigger and the deflection of the beam is taken by the camcorder. The pulling force is obtained by the tensile test machine and the deflection is obtained by the vision analysis program (Proanalyst). The force and the deflection of the passive trigger component is plotted as shown in Figure IV. 2 (b). The characteristic modulus of the composite materials is computed in 0.93 Gpa and the modeling results match well as the graph in Figure IV. 2 (b). Using the model, we can design the triggering force of the passive trigger when it meet the required deflection for triggering. The

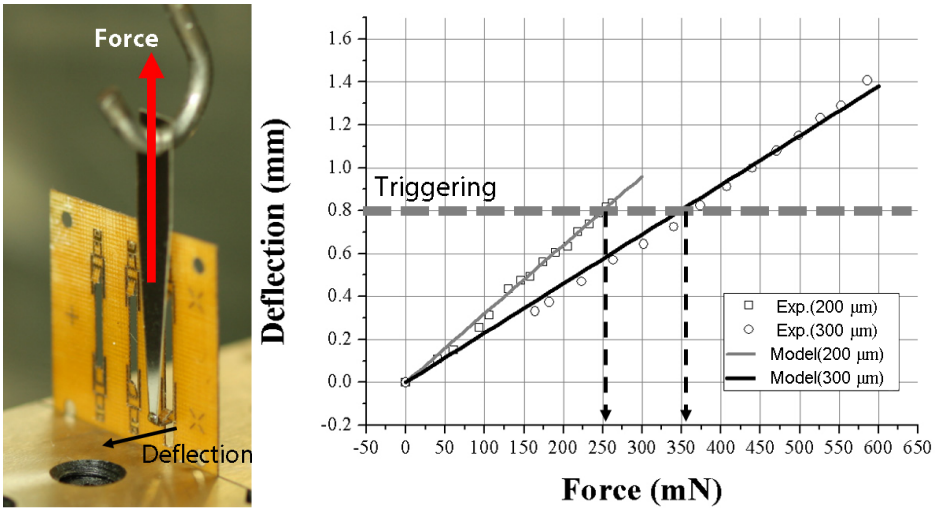

(a) (b)

Figure IV. 2 (a) the passive trigger specimen for tensile experiments and the experimental setup, (b) the experiment results and compare to the model developed by obtaining the characteristic modulus of the composite material.

required deflection is determined by the initial body angle, θ. The prototypes have same initial angle of 32° which value correspond to 0.8mm in the desired deflection. Finally, the stiffness of the actuator, *k*, can be calculated by dividing the stroke of the actuators to the triggering force.

$$Actuator\ Stiffness\,(k) = \frac{Triggering\ Force\,(F)}{Actuator\ Stroke\,(s)}$$

IV.1.2 Simulation Results of Jumping on Ground

From the dynamic modeling, kinetic and kinematic data including the reaction force and the takeoff velocity are simulated. Simulation with various design parameters are performed and the representative results are plotted in Figure IV. 3. As shown in Figure IV. 3, stiffness of the actuator changes the takeoff velocity as well as the maximum reaction force while the leg length

changes only the maximum reaction force. Takeoff times are changed by both parameters. Therefore, the jumping velocity can be changed by actuator stiffness and the maximum reaction force can be tuned by the length of leg.

When stoke of the actuator is fixed, the stiffness of the actuator determines the amount of the elastic energy stored in actuator. Therefore, the stiffness of the actuator changes the final takeoff velocity as shown in Figure IV. 3 (a). We can increase the takeoff velocity by using the actuator that has high stiffness. In this research, the stiffness of the actuator is determined by the triggering force of the compliant trigger as described in previous section.

If the stored elastic energy is constant, the takeoff velocity does not change by various leg lengths as Figure IV. 3 (b). It means that the leg length is not related with mechanical efficiency of the robots. The leg length effects to the reaction force profile. As the leg length increases, the maximum reaction force decreases and the takeoff time is delayed. The low reaction force reduces the stress exerted on the legs. However, too long legs induce the weight increase and the takeoff velocity decreases eventually.

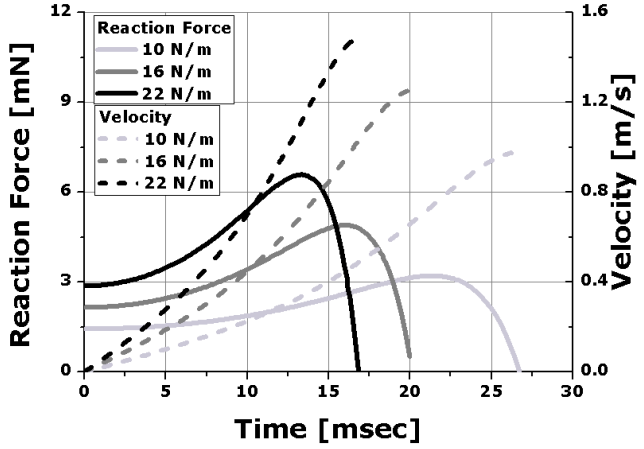

(a)

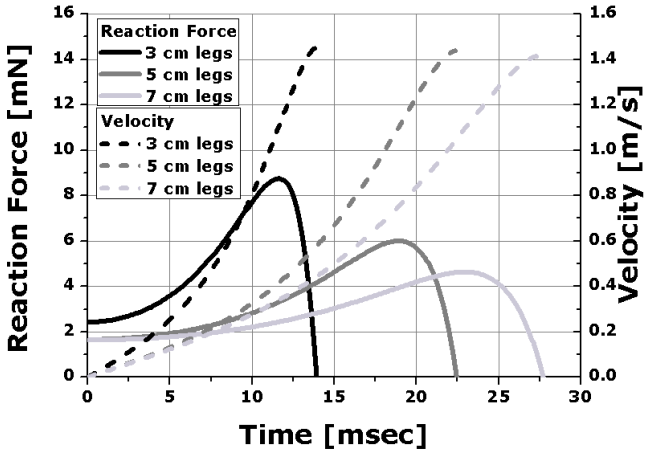

(b)

Figure IV. 3 Simulation results of jumping on ground. Reaction force and velocity profiles depend on various stiffness of the actuator (a) and leg lengths (b)

IV.1.3 Dynamic Modeling of Jumping on the Water Surface

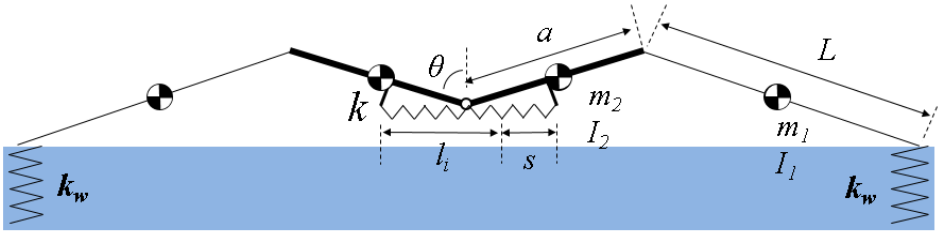

Figure IV. 4 Dynamic model of the robotic water strider jumping on water

As described in previous bio-hydrodynamic force section, the surface curvature force is dominant reaction force that endures the driving force of the robot legs. The curvature force is modeled as an elastic force which is linearly increased depending on sinking depth until the water surface is not broken. Therefore, Lagrange's differential equation (10) can be derived with following energy equation unlike jumping on the ground.

$$T = \sum \frac{1}{2} m_i v_i^2 + \sum \frac{1}{2} I_i w_i^2$$
$$V = \frac{1}{2} k s^2 + \sum \frac{1}{2} m_i g h_i + \frac{1}{2} k_w d^2$$

where k_w is the stiffness of the water surface, d is the sinking depth of the legs. k_w varies depending on the length and the shape of the submerged part of the legs. Other parameters are same with the ground jumping model as shown in Figure IV. 4.

In order to obtain the value of the water surface stiffness, experiments are performed, and we measure the force and the sinking depth by using the

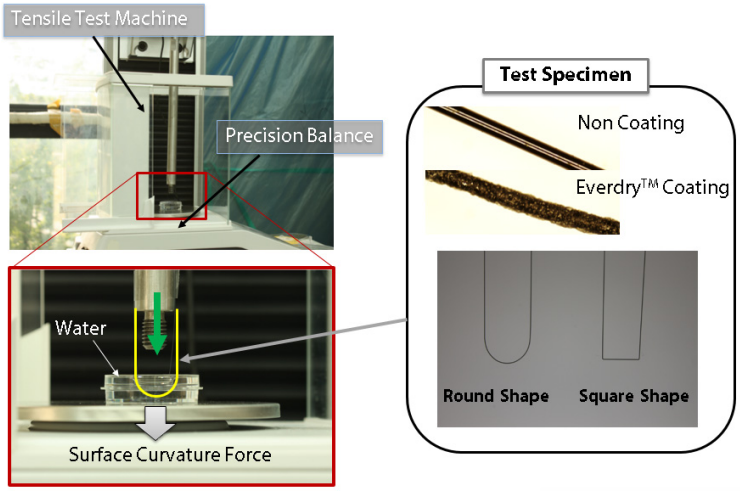

Figure IV. 5 Experimental setup for measuring the surface curvature force of the leg tip

precision balance and the tensile test machine. Two kinds of leg shapes are prepared to measure the stiffness of the water surface. Furthermore, the effect of super hydrophobic coating can be measured with the experiments. The round shape and the square shape of the superelastic SMA wire with non-coated and hydrophobic coated surface treatment in each shape are prepared as test specimens as shown in Figure IV. 5.

The sinking depth is measured and controlled by the tensile test machine that has metallic bar that the specimens are attached at. When the specimen start to push down the water surface, the precision balance measure the increment of the weight which is the amount of the curvature force.

Shape of the leg submerged in the water surface should be carefully designed to have large curvature force without breaking the water surface and it affect the reaction force profile through the sinking depth. Initially, the legs are designed as a straight wire that is bent at the end tip to block the propagation of penetrating the water surface starting from the end of wire as shown in the upper

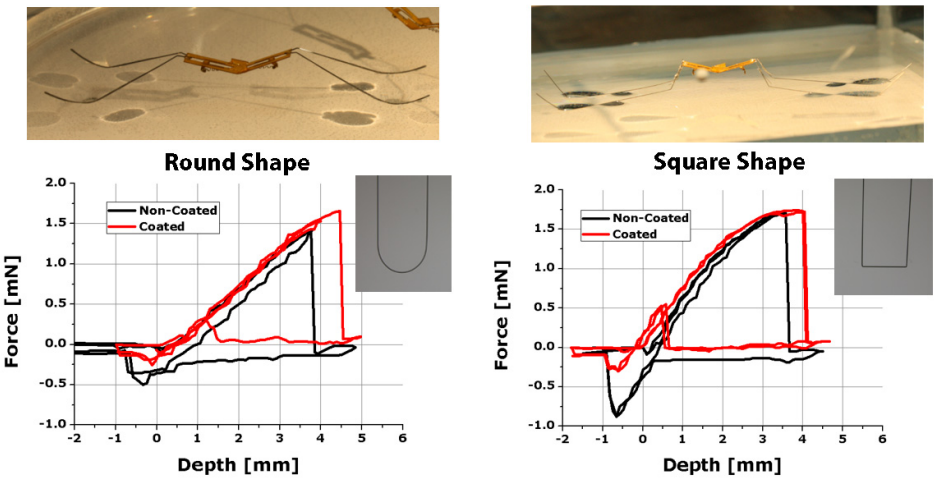

(a) (b)

Figure IV. 6 Experiment results of measuring the stiffness of the water surface

right picture of Figure IV. 6. However, the angled leg tip causes unpredictable contact condition between the legs and the water surface because the robot rotate the legs and the angle between legs and the surface changes continuously. In order to maintain the uniform shape of the contact surface while the legs are swinging, the leg tip is designed as round shape. As rotating the legs, the round shape leg tip as shown in upper left picture of Figure IV. 6, maintains the round shape of the contact surface with the water.

Figure IV. 6 shows the result of measuring the surface curvature force. Both graphs show that the curvature force increases as the sinking depth increases and the force drops suddenly at the certain depth. The force drop occurs when the water surface is broken and the specimens are immerged in the water. The round shape specimen have quite linear force profile through the sinking depth while the square shape specimen have nonlinear relationship at around maximum depth.

Hydrophobic coating increases the maximum force and the depth. In case

of the round shape specimen, hydrophobicity affect more than the square shape specimen as shown in graphs. The graph shows the other advantages of hydrophobic coating when the specimen escape from water. In both graphs, less negative force are found if the specimen is coated. The resulting stiffness of the water surface and the maximum forces are listed in Table IV. 1.

We decide to apply the round shape legs to the robot design because it shows linear stiffness characteristics and constant contact surface shape for minimizing the error in dynamic modeling.

Table IV. 1 The stiffness of the water surface and the maximum curvature force

Parameters		Round Shape	Square Shape
Stiffness of the Water Surface	Non Coating	0.375 N/m	Nonlinear
	Coating	0.375 N/m	Nonlinear
Maximum Surface Curvature Force	Non Coating	0.057 N/m	0.08 N/m
	Coating	0.07 N/m	0.08 N/m

IV.1.4 Modeling of Curvature Force on Legs

The curvature force is the dominant force for locomotion on water [17-20, 23]. We measured the curvature force around the leg of the robotic water strider experimentally as described in previous section. The round shape of the leg shows linear relationship between the curvature force and depth. The shape of the leg effect the resulting curvature force by varying the depth along the submerged legs. Actually, real water striders have flexible legs and the legs are bent when they float and move on water. The curvature force around the circular cylinder bent on the water surface have been studied and the curvature force can be computed analytically [44, 45]. Based on these research, we can compute the

curvature force around the leg of the robotic water strider as the experimental measurements.

If the radius of the circular cylinder is small enough to ignore the buoyancy, the cross section of the water surface around the cylinder is deformed as Figure IV. 7. The curvature force per unit length, f_c, is simplified as following equation [45].

$$f_c(h) = 2\rho g l_c \cdot d\sqrt{1-(d/2l_c)^2} \tag{12}$$

$$l_c = \sqrt{\frac{\gamma}{\rho g}}$$

where ρ is density of water, g is gravitational acceleration, d is depth of the center of the cylinder beneath the free surface of water and l_c is the capillary length of water.

With this equation, we can compute the resulting curvature force of the legs with different shapes. The resulting curvature force, F_c, is integration of the curvature force per unit length along the submerged length, l_w, and it

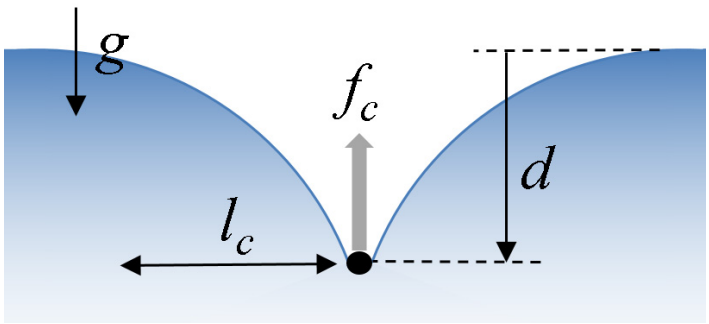

Figure IV. 7 Cross section through a circular cylinder floating on the water surface

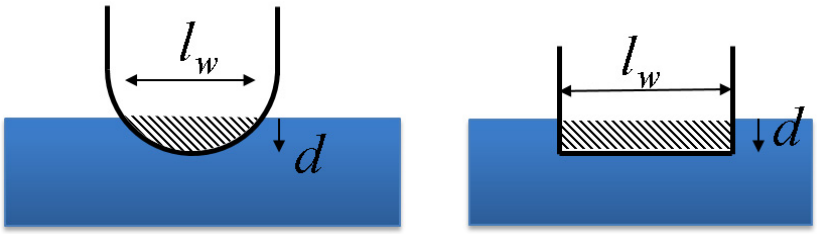

Figure IV. 8 Two shapes of the legs for the curvature force modeling.

corresponds with the area deformed by the legs as shown Figure IV. 8.

$$F_c(d) = \int f(d)\, dl_w \tag{13}$$

The analytical curvature force profiles and the experimental results of two shape of legs are plotted together in Figure IV. 9. We can find the linearization of the curvature force through the sinking depth in the graph of the round shape leg as shown in Figure IV. 9 (a). However, the little drop of the curvature force is seen in results of round shape leg data while the modeling and experiments match well in results of square shape leg case. The errors are caused by the difference between submerged length of modeling and experiments. As shown in Figure IV. 10, the submerged length is decreased slightly at the round shape leg. Compared to the square shape specimen, the round shape specimen have dimple effect at the end of the submerged wire as Figure IV. 10 (a). That causes that the curvature force is little lower than analytical modeling. In contrast, the experimental results of the square shape specimen match well with the analytical modeling because the submerged part of the square shape wire have equal depth and the integration of the curvature force along the submerged length is fully

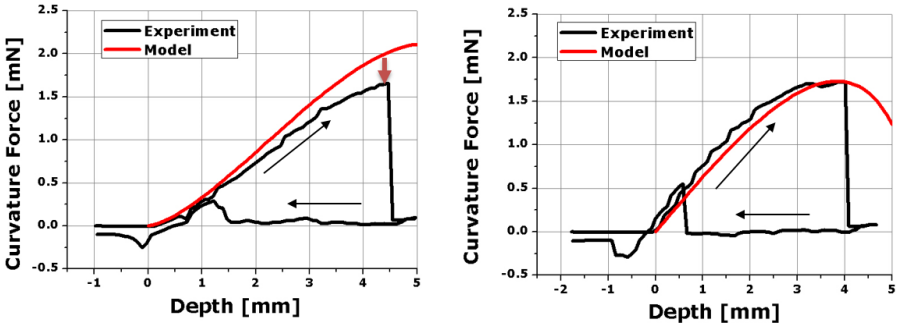

(a) (b)

Figure IV. 9 The analytical modeling and experimental measurement of the curvature force of round shape leg (a), and square shape leg (b)

exerted on the specimen. As experimental results, the curvature force of the square shape leg have nonlinear relationship with sinking depth.

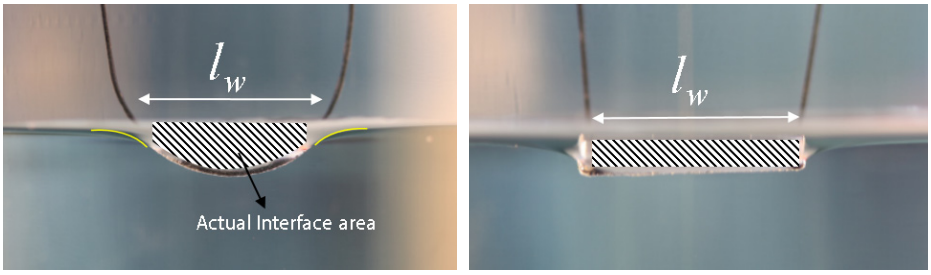

(a) (b)

Figure IV. 10 Side view of experimental measurement of the curvature force. (a) round shape leg, (b) square shape leg

With round shape leg, we can obtain the linear stiffness of the water surface interacting with the legs. The curvature of the round shape legs would change the stiffness of the water surface and the maximum reaction force can be changed. In this thesis, the radius of the curvature is 6mm and the stiffness of the water surface is 0.375 N/m as experimental and analytical results.

IV.1.5 Simulation Results of Jumping on Water

The dynamic simulation of jumping on water is performed with properties of the robot and the water surface measured experimentally. Kinetic and

kinematic data including the reaction force, the sinking depth and the takeoff velocity are simulated. Simulation with various design parameters are performed and the representative results are plotted in Figure IV. 11. As shown in Figure IV. 11, stiffness of the actuator changes the takeoff velocity as well as the maximum reaction force while the leg length changes only the maximum reaction force. Takeoff times are changed by both parameters. Therefore, the jumping velocity can be changed by actuator stiffness and the maximum reaction force can be tuned by the length of leg. The simulations are performed with the assumption that the water surface endures the reaction force as much as the robot generates. However, the water surface would be broken when the reaction force exceeds the maximum curvature force, which is the design criteria of the robotic water strider. Therefore, the leg length is properly designed to reduce the reaction force below the maximum curvature force after the actuator stiffness and power is determined.

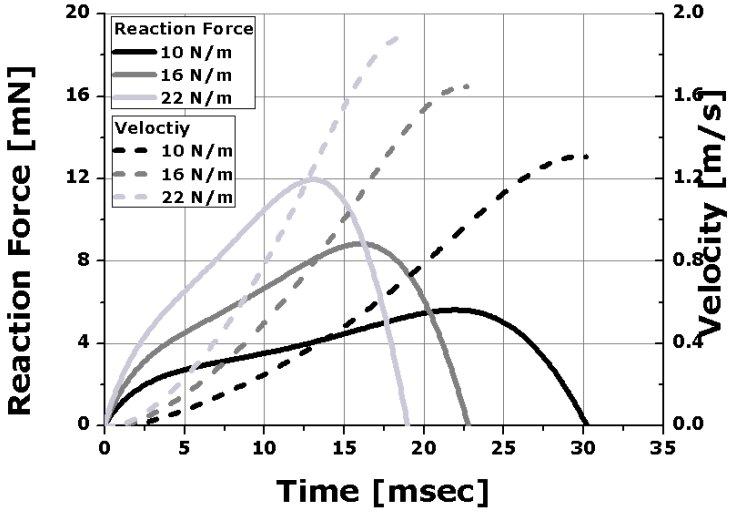

(a)

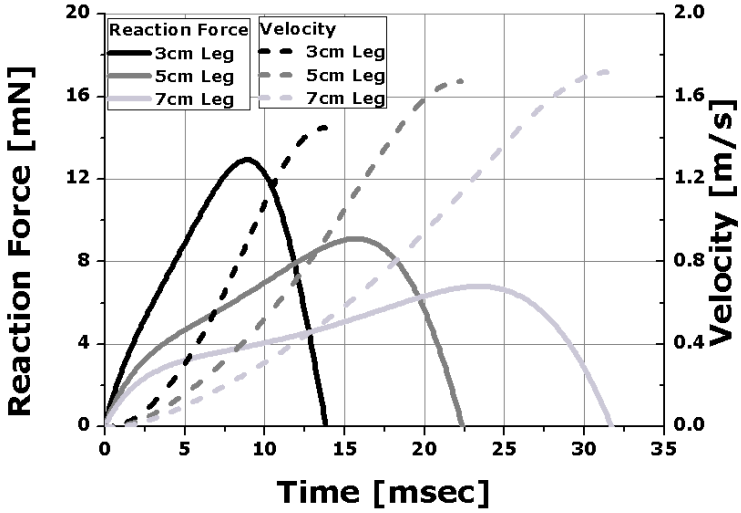

(b)

Figure IV. 11 Simulation results of jumping on water. Reaction force and velocity profiles depend on various stiffness of the actuator with a constant leg length of 5cm (a) and various leg lengths with a constant stiffness of 16 N/m (b).

IV.2 Jumping Experiments

The various robot prototypes that have different design parameters are tested on both the ground and the water surface. The jumping motions are took by high-speed camera with 3000 fps in frame speed.

Five prototypes of the robotic water striders are built as shown in Figure IV. 12. The prototypes have two different leg length in 3cm, 5cm, and various actuator stiffness by changing triggering force and actuator stroke. The specifications of prototypes are listed in Table IV. 2.

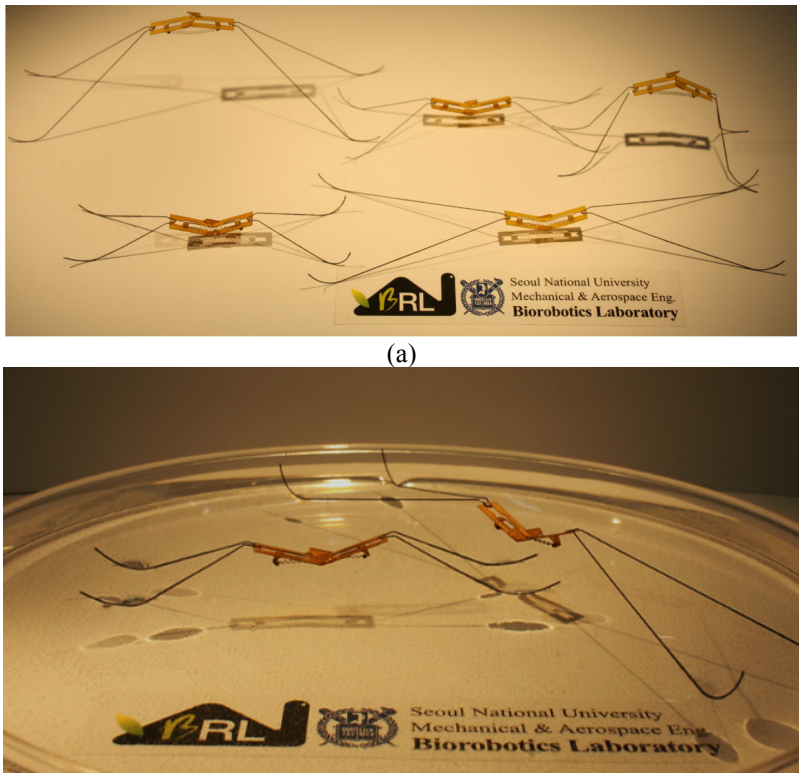

(a)

(b)

Figure IV. 12 (a) Robotic water striders that have various leg length and actuation stiffness. (b) Robotic water striders floating on water

Table IV. 2 Specifications of the robotic water strider prototypes

	Robot #1	Robot #2	Robot #3	Robot #4	Robot #5
Leg length [cm]	3			5	
Triggering force [mN]	95	201	118	95	118
Actuator stroke [mm]	5.75		4.5	5.75	
Actuator stiffness [N/m]	16.52	35	26	16.52	20.5
Initial angle of the body [°]	32				
Width of Passive Trigger Cantilever [μm]	200		250	200	
Composite Thickness [μm]	170	240	170		

The prototypes have different triggering forces and actuator stiffness, so the actuators are triggered at different temperatures. Thin heat wire (NiCr wire) is put under the robots and heated by applying electric current. As increasing the temperature, the stiffness of the SMA actuator is increased until the force meets the required triggering force. The convection heat of the heat wire is enough to rise the temperature above 120 °C which value is much higher than the transition temperature of the SMA actuator, 20 °C in no loading condition. When the heat wire heat the actuator, both the force and transition temperature of the actuator are increased and finally the required actuation force can be achieved. With the NiCr wire of 3 mil. diameters and the electric current of 0.8 A, the robot is triggered in a second.

IV.2.1 Jumping on Ground

Jumping experiments on ground are performed with prototypes described in previous session. The experiment would show the performance of the robots and compare to the dynamic modeling so that the results can verify the reliability of the modeling.

Following figures show the experimental results including the sequential pictures taken by the high speed camera, the velocity of the robot prototypes

obtained by vision analysis, and the modeling simulation result plots. The results of five robot prototypes are shown in Figure IV. 13 to Figure IV. 17.

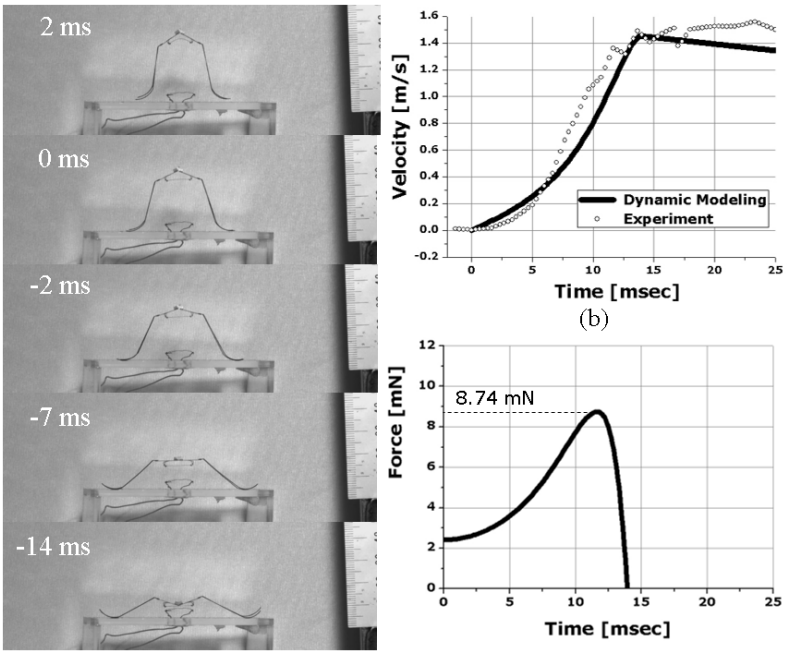

(a) (b) (c)

Figure IV. 13 The experimental and simulation results of Robot #1. (a) sequential pictures taken by the high speed camera (b) velocity (c) reaction force.

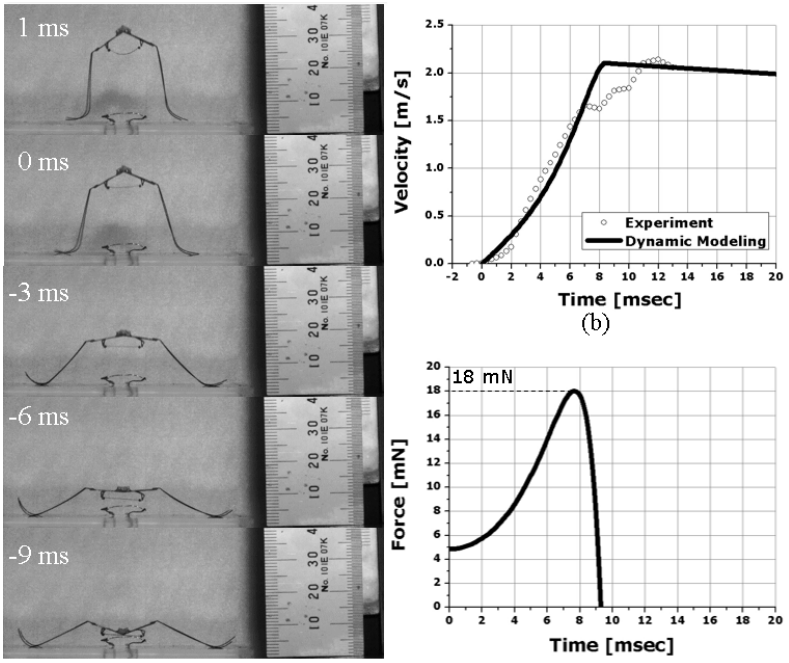

Figure IV. 14 The experimental and simulation results of Robot #2. (a) sequential pictures taken by the high speed camera (b) velocity (c) reaction force.

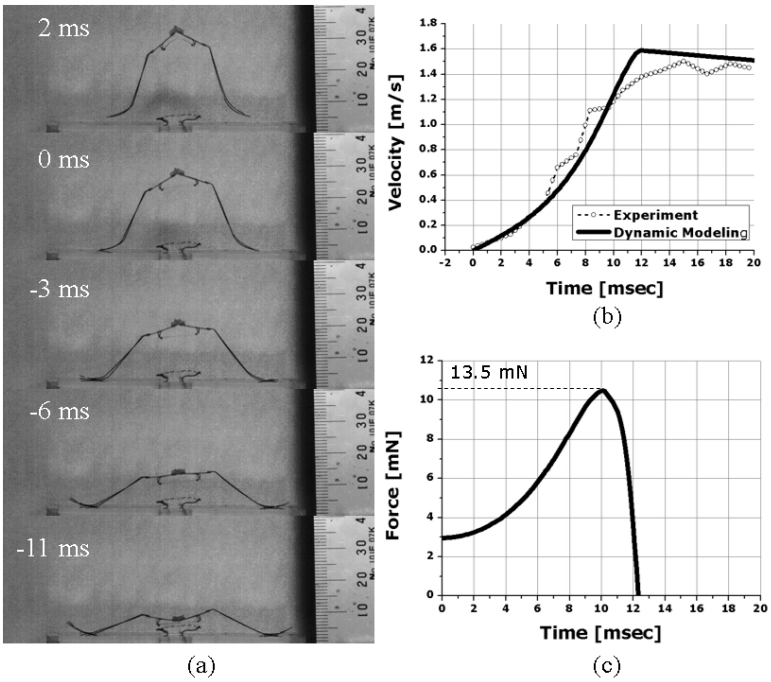

Figure IV. 15 The experimental and simulation results of Robot #3. (a) sequential pictures taken by the high speed camera (b) velocity (c) reaction force.

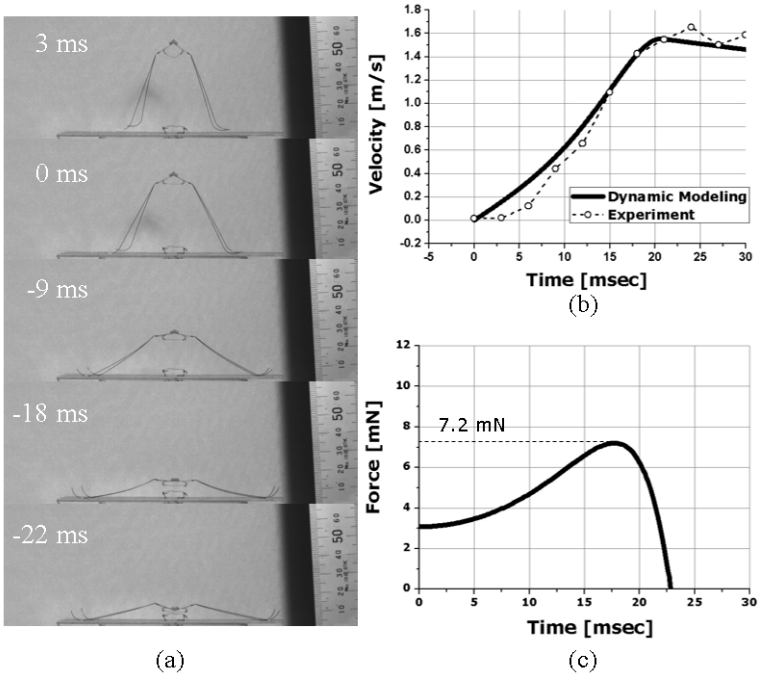

Figure IV. 16 The experimental and simulation results of Robot #4. (a) sequential pictures taken by the high speed camera (b) velocity (c) reaction force.

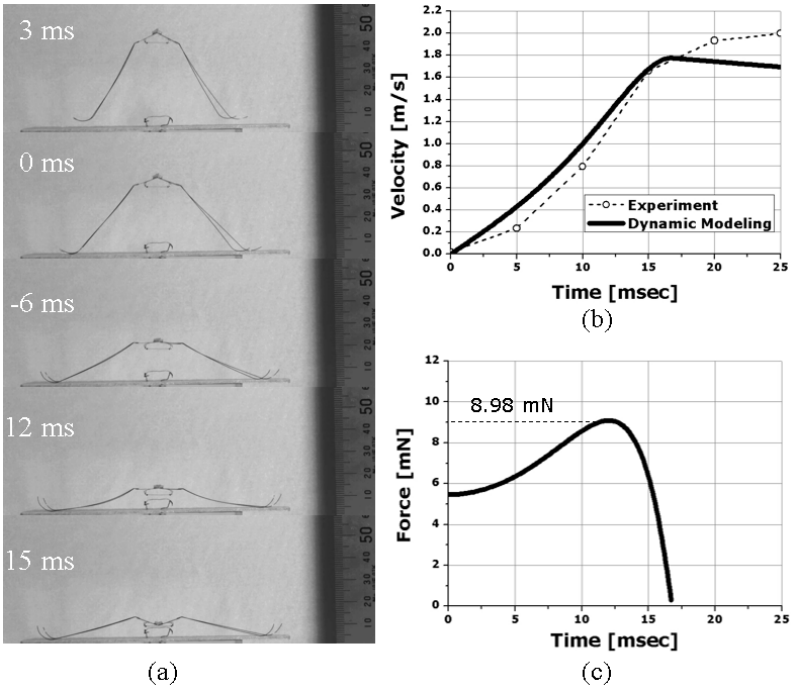

Figure IV. 17 The experimental and simulation results of Robot #5. (a) sequential pictures taken by the high speed camera (b) velocity (c) reaction force.

The velocity graph, (b), in each figure shows the center of mass velocity plotted by vision analysis and simulation from the dynamic modeling. Five results of experiments and simulation match well as shown in each graph. Therefore, the dynamic modeling can be verified and it is reliable to predict the robot behavior. From the modeling, the reaction forces exerted to the legs and ground are calculated when the robots take off. As the design parameters change, the resulting takeoff velocity and the maximum reaction force are varied as listed in Table IV. 3.

Table IV. 3 Experimental and Modeling Results of Jumping on Ground

	Robot #1	Robot #2	Robot #3	Robot #4	Robot #5
Leg length [cm]	3			5	
Actuator stiffness [N/m]	16.52	35	26	16.52	20.5
Max. Reaction Force [mN]	8.74	18	13.5	7.2	8.98
Experimental Takeoff Velocity [m/s]	1.45	2.1	1.48	1.53	2
Dynamic Modeling Takeoff Velocity [m/s]	1.45	2.11	1.6	1.62	1.9

As result data, the maximum reaction force increase linearly depending on the actuator stiffness. The leg length affect to the reaction force and the takeoff velocity. Longer leg length has less maximum force and higher takeoff velocity. Less maximum reaction force is resulted by longer moment arm of long leg with same torque generated by body mechanism and resulting velocity is amplified by long leg.

The relationship between the maximum reaction force (peak force) and the takeoff velocity can be calculated using both dynamic modeling and the energy method express as equation (7). In energy method, the mechanical efficiency of different leg length prototypes is 17% of 3cm leg and 30% of 5cm leg each other,

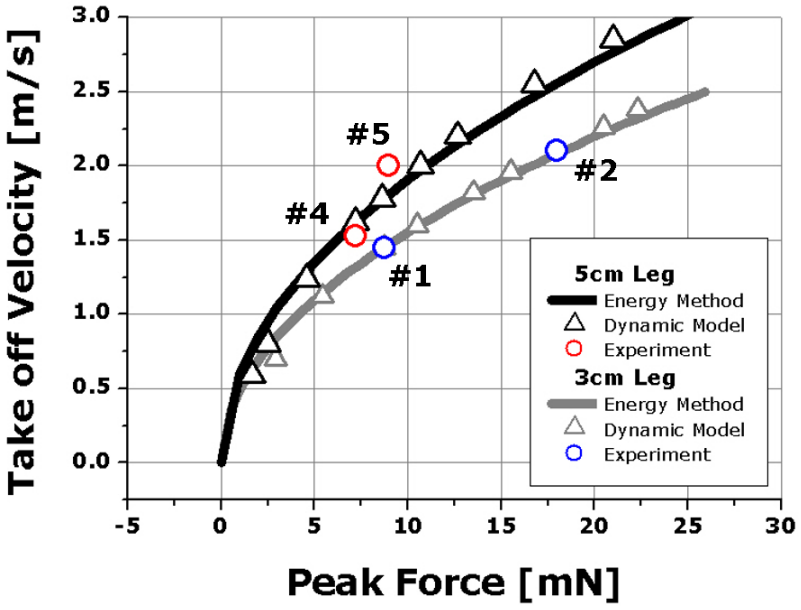

Figure IV. 18 the relationship between the peak force and the takeoff velocity by obtaining from the energy equation and the dynamic modeling. The experimental results are put on the graph and match well with computed data.

measured by experiments. Two computed results and experiment results match well as shown in Figure IV. 18.

As shown in result graphs, the modeling data and the experimental data match well enough to estimate the robot performance using modeling. Surprisingly, the modeling has no fitting technique to match with experiments except for trigger timing. The error can be minimized because the robot structure is very simple and the flexure hinge mechanism might minimize the friction.

As a result of jumping on ground, the robot can jump higher as the actuator is stiffer and stronger and the reaction force is higher as much as the robot structure can endure.

IV.2.2 Jumping on the Water Surface

Jumping experiments on the water surface are performed with prototypes which are used on ground jumping experiments. The experiment would show the performance of the robots on water and compare to the dynamic modeling with the water surface modeling and the results can verify the reliability of the modeling.

Following figures show the experimental results including the sequential pictures taken by the high speed camera, the velocity of the robot prototypes obtained by vision analysis, and the modeling simulation result plots. The results of five robot prototypes are shown in Figure IV. 19 to Figure IV. 23.

The dynamic modeling includes the elastic model of the water surface. The velocity, the reaction force, and the sinking depth of the legs are obtained by simulation. The parameters used in model is described in previous section.

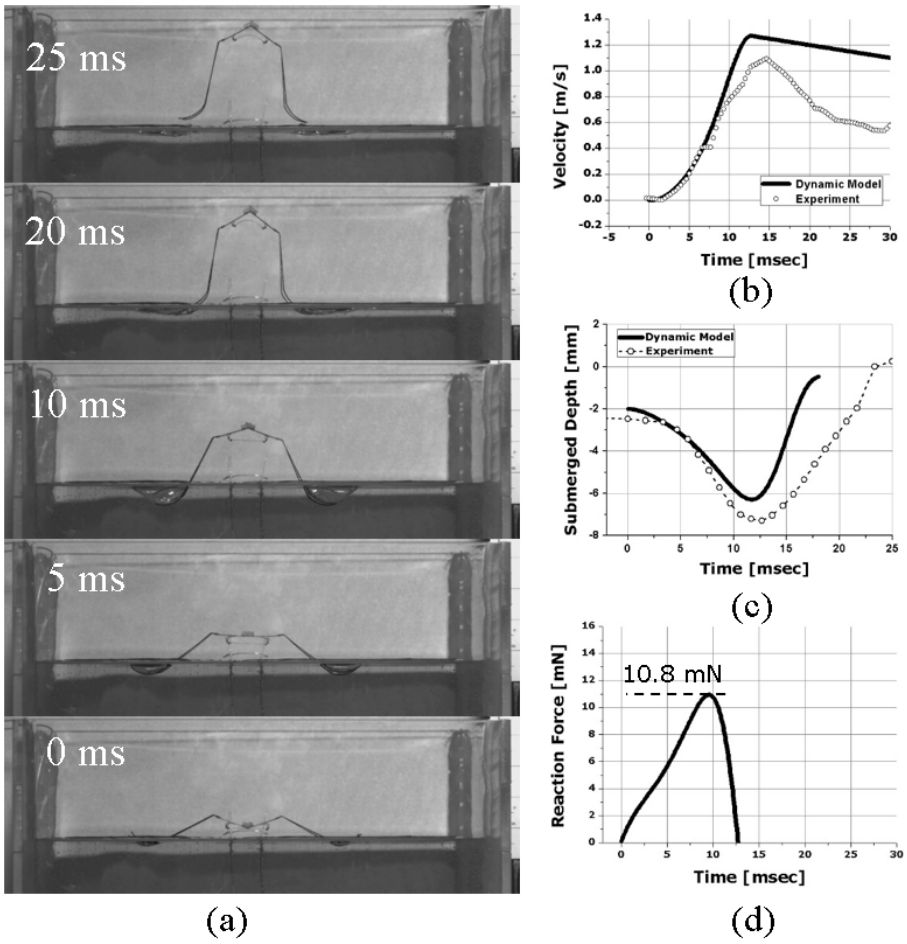

Figure IV. 19 The experimental and simulation results of Robot #1 on water. (a) sequential pictures taken by the high speed camera (b) velocity (c) submerged depth (d) reaction force

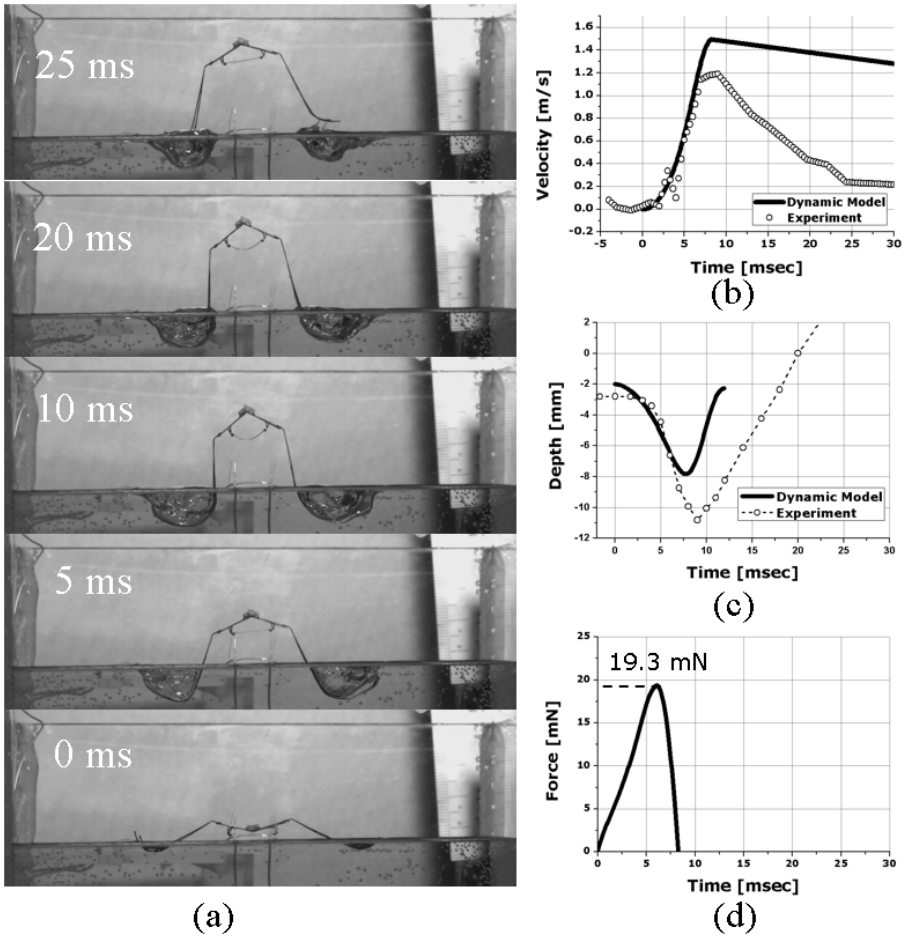

Figure IV. 20 The experimental and simulation results of Robot #2 on water. (a) sequential pictures taken by the high speed camera (b) velocity (c) submerged depth (d) reaction force

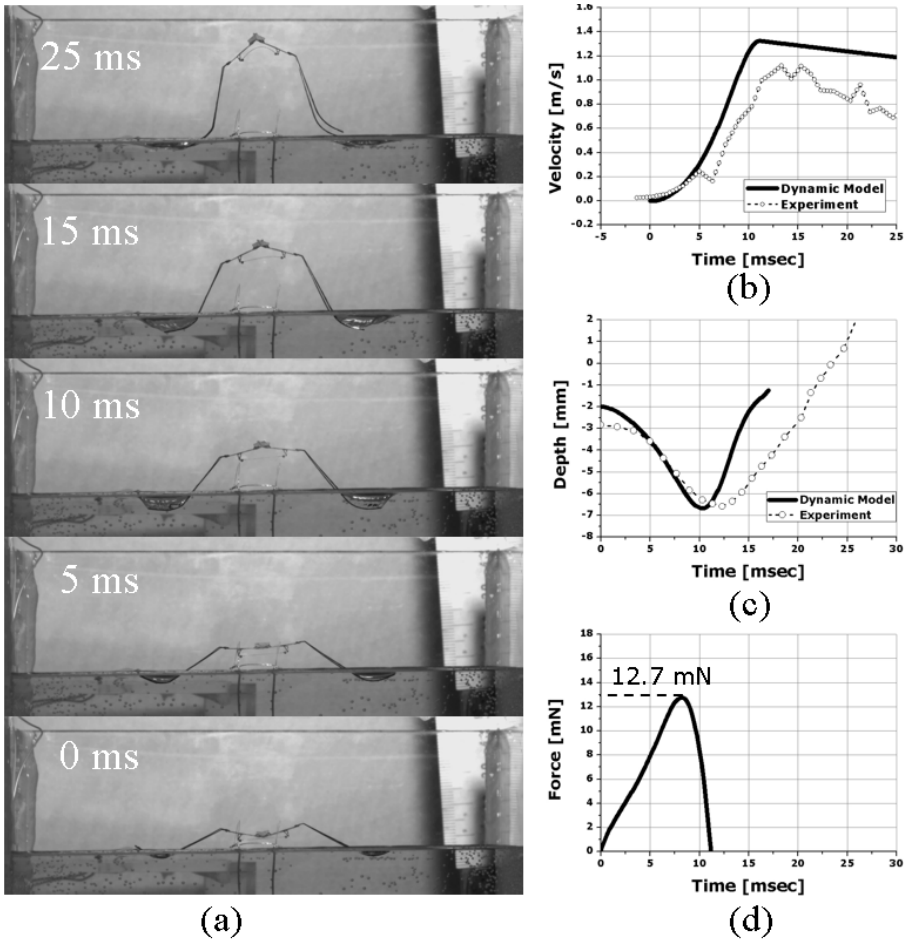

Figure IV. 21 The experimental and simulation results of Robot #3 on water. (a) sequential pictures taken by the high speed camera (b) velocity (c) submerged depth (d) reaction force

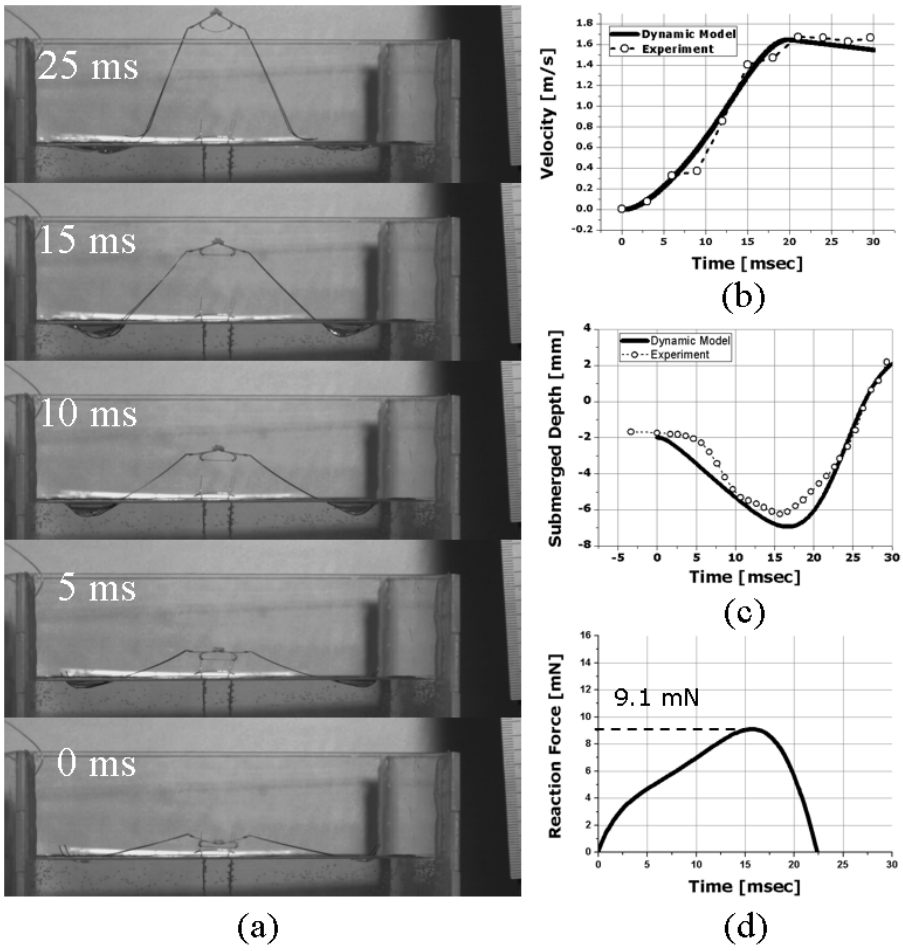

Figure IV. 22 The experimental and simulation results of Robot #4 on water. (a) sequential pictures taken by the high speed camera (b) velocity (c) submerged depth (d) reaction force

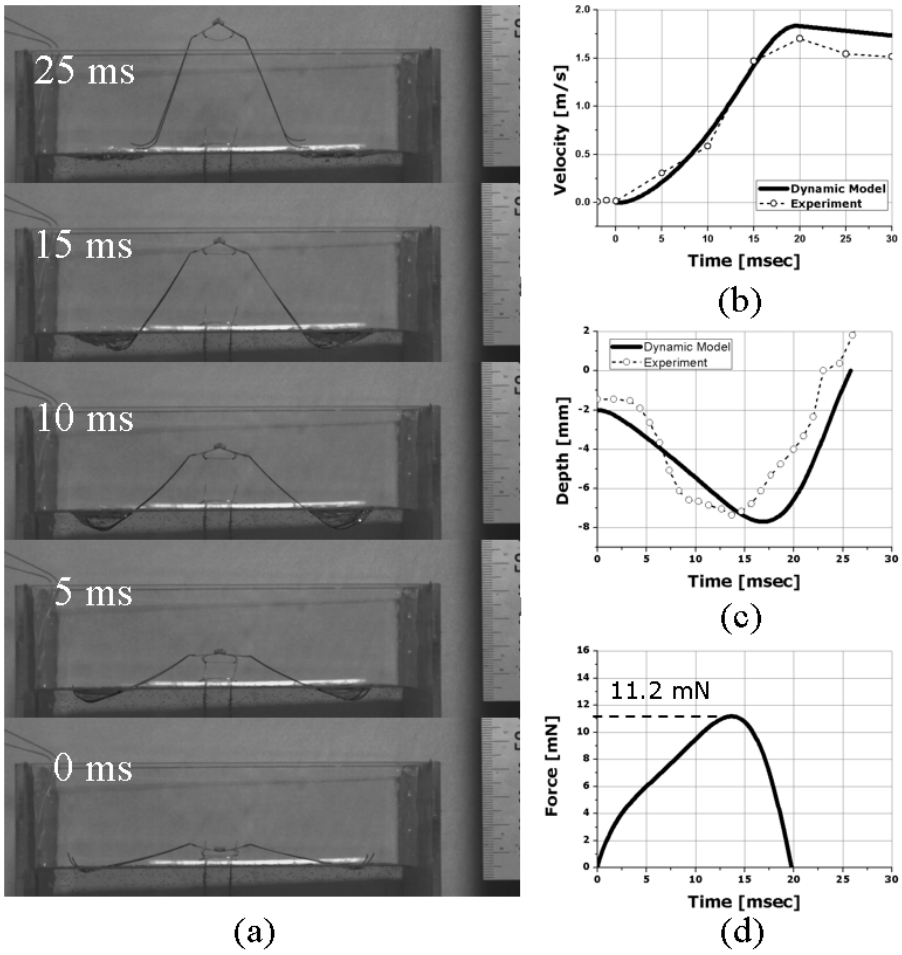

Figure IV. 23 The experimental and simulation results of Robot #5 on water. (a) sequential pictures taken by the high speed camera (b) velocity (c) submerged depth (d) reaction force

As shown in result graphs, the robot prototypes #1, #2, #3, #5 cannot follow the modeling plots. At the right after triggering, the velocity follow the simulation well, but suddenly the experimental velocity drop rapidly faster than gravitational acceleration. Therefore, we can assume the driving legs penetrate the water surface and the robot cannot get enough reaction force to obtain takeoff velocity as much as the value in modeling.

As described in chapter II, we have design criteria of water jumping robot that the reaction force should be below the maximum surface tension. The results are plotted on the graph about the relationship between the peak force and the takeoff velocity as shown in Figure IV. 24. As shown in the graph, the robots that has higher peak force than certain force such as robot #1, #2, #5 do not achieve takeoff velocity calculated by modeling and energy method. However, robot #4 achieves the takeoff velocity exactly same as modeling. Moreover, the sinking depth of the legs can follow the modeling data quiet well as shown in Figure IV. 22 (c). Therefore, we can assume the robot #4 does not break the water surface and smoothly leap out of the water surface.

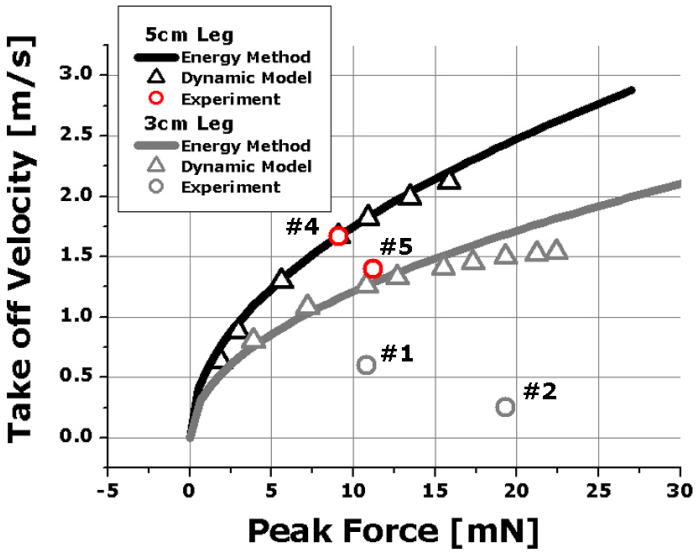

Figure IV. 24 Modeling and experimental Results of the takeoff velocities on water depends on the driving peak force

To verify the design criteria, the peak force is divided by submerged length of the legs. The maximum submerged length is measured by the video analysis and the 5cm-leg prototypes have around 16.5 mm and 3cm-leg prototypes have around 12.2mm. By dividing the submerged length to the peak reaction force, the results are plotted with the parameter of the reaction force per submerged length as Figure IV. 25.

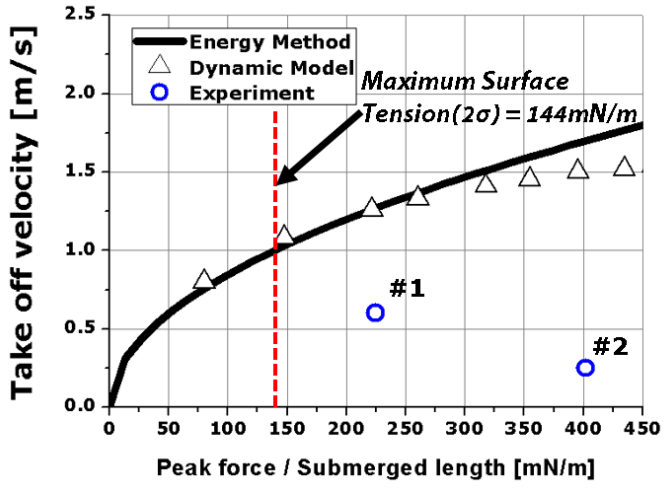

(a)

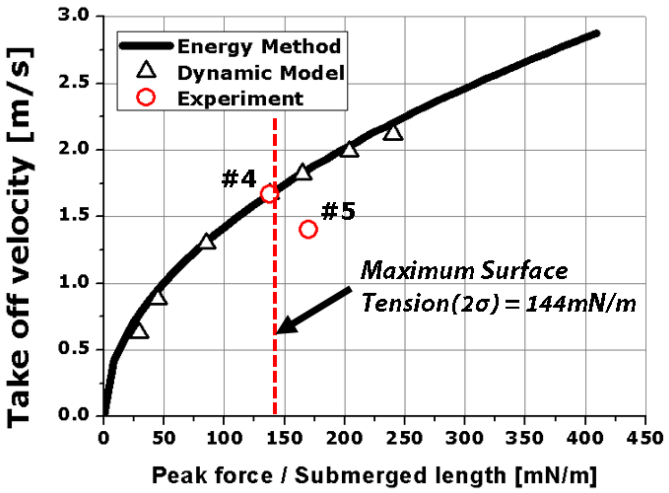

(b)

Figure IV. 25 The modeling and experimental results plotted on the graph of the takeoff velocity versus the peak reaction force per submerged length. (a)3cm-leg prototypes (b)5cm-leg prototypes

IV.3 Hydrodynamic Forces in Jumping on Water

In section II.3.2, rough estimation of the hydrodynamic forces in jumping on water were calculated and the curvature force is the dominant force exerted on the driving leg of the water striders. With experimental data, the hydrodynamic forces generated by the robotic water strider can be calculated.

Each term of hydrodynamic forces is expressed as (1), and the drag term is modified to obtain more accurate quantity by adding the drag coefficient (C_D). Typical drag coefficient of the circular cylinder is 1.1 [46]. The reaction force on the water surface is summation of entire hydrodynamic forces as following equation (14).

$$|F_r| = \frac{1}{2} C_D \rho U^2 A + \rho g h A + \rho V \frac{dU}{dt} + \mu U \frac{1}{w} A + \sigma \frac{1}{w} A \qquad (14)$$

The legs of the robotic water strider show the lateral motion as well as the vertical motion as shown in Figure IV. 26, the picture of the tracking points. We measured the velocity and acceleration in vertical and lateral directions that is needed to calculate all hydrodynamic forces exerted on legs. Geometrical values such as projection area and contact length are measured and hydrodynamic force is computed separately in these two coordinates as Figure IV. 27.

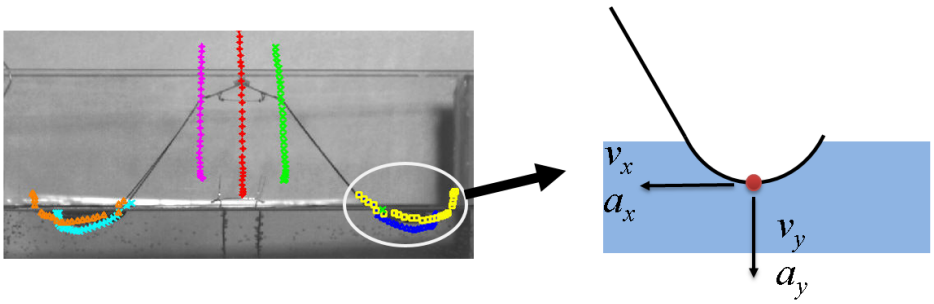

Figure IV. 26 The tracking points of the robotic water strider jumping on water. The legs have the vertical and lateral motion during takeoff.

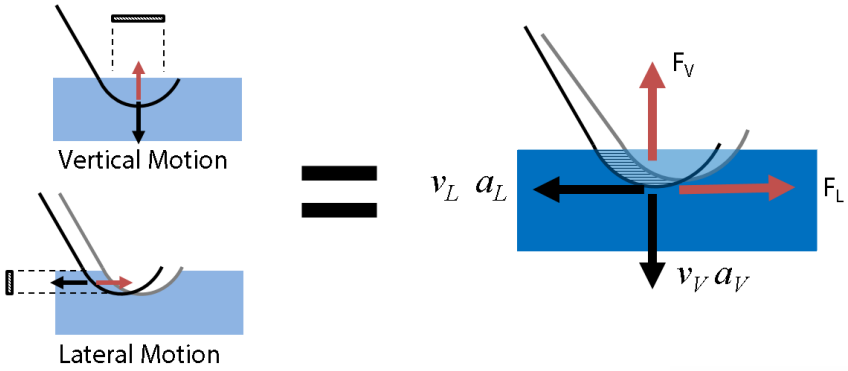

Figure IV. 27 Vertical and lateral motion of the legs. Separated measurements of the

Using the video analysis with the high speed video of the robot #4 which satisfies the design criteria, the velocity, acceleration, projection area in vertical and lateral direction are measured and all hydrodynamic forces in equation (14) are calculated along the takeoff time. Figure IV. 28 shows hydrodynamic forces change while the robot takes off the water surface. As shown in the graph, the curvature force is the largest force that is used as the reaction force for obtaining enough vertical momentum. Other forces are negligible, but the drag forces are the secondary dominant forces that may effect to jumping. Especially, the lateral drag force have considerable quantity, but it is lateral force that is perpendicular to the vertical jumping direction. It is hard to calculate how much this lateral force effects to vertical direction force precisely. We can estimate the vertical force induced by the lateral drag force roughly by employing the lift/drag coefficient in aerodynamic analysis. Generally, the lift/drag coefficient is below 1, and we can estimate that the vertical lift would be smaller than the quantity of the lateral drag force. In this graph, the curvature force is enough to generate the reaction force of dynamic simulation result for the robot to get the takeoff

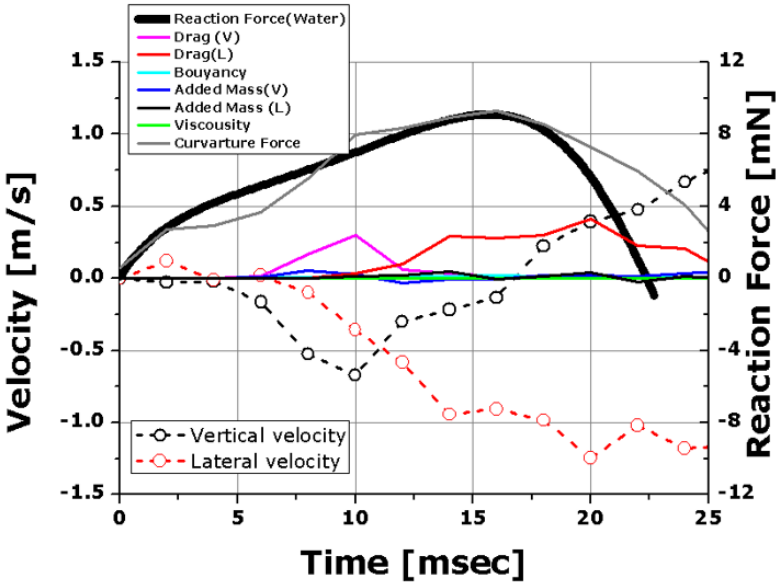

Figure IV. 28 Vertical and lateral velocity of the submerged leg of the robotic water strider (dotted lines). Hydrodynamic forces exerted on the leg (colored solid lines). The reaction force simulated by the dynamic modeling (Black thick solid line)

velocity measured by experiments. That means that other forces hardly effect to jumping performance.

To compare the experimental results with the rough calculation of hydrodynamic forces in previous chapter II.3.2, the percentage of hydrodynamic forces are plotted in the column chart as Figure IV. 29. In the experimental result, 75.4% of the total hydrodynamic force is generated by the surface curvature force induced by the surface tension of water. The drag force is secondary dominant force that is generated more than rough calculation. If the water surface is broken, the robot loses the largest force for jumping. Therefore, the design criteria for efficient jumping is that the driving force should be below the maximum curvature force of the water surface as described in previous chapter.

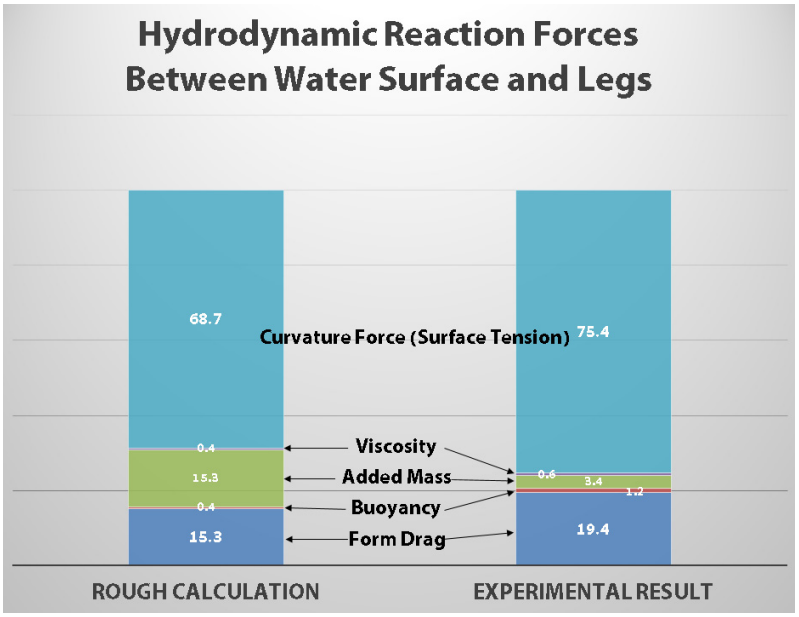

Figure IV. 29 Percentages of hydrodynamic forces. Rough calculation with parameters of the water striders (left column) and parameters measured with the robotic water (right column)

IV.4 Water-Ground Velocity Ratio

Water jumping performance can be evaluated by comparing with the takeoff velocity on ground. The water-ground velocity ratio is defined as follows.

$$\text{Water-Ground Velocity Ratio}\,(\varepsilon_w) = \frac{\text{Take off Vel. on Water}}{\text{Take off Vel. on Ground}} \quad (15)$$

On ground, the reaction force can be obtained from ground as much as the robot generates. However, the reaction force on water might drop when the driving legs penetrated the water surface. We assumed that the legs penetrate the water surface when the driving force exceeds the maximum curvature force of the water surface (2σ) as criteria inequality (9) in chapter II. 4.

The surface tension of water (σ) is 72 mN/m which value is inherent property of water. Therefore, the reaction force per submerged length should not exceed the value of 144 mN/m for legs not to penetrate the water surface. We can verify the criteria with the graph that plot the experimental results with the water-ground velocity ratio through various reaction force per submerged length as Figure IV. 30. The water-ground velocity ratio start to decrease when the reaction force per submerged length exceed the maximum curvature force. It means that the legs penetrate the water surface and lose the largest force which is the curvature force. That causes the sudden drop of momentum transfer to the robot.

Therefore, maintaining the reaction force per submerged length below the maximum curvature force is critical for efficient jumping on water with maximizing momentum transfer to the robot. As the result of the robot #4, it has almost similar takeoff velocity on water with jumping on ground. It can jump on water as it jumps on rigid ground. In that case, large waves and splash around the driving legs are hardly observed and it means that the momentum transfer to water is minimized.

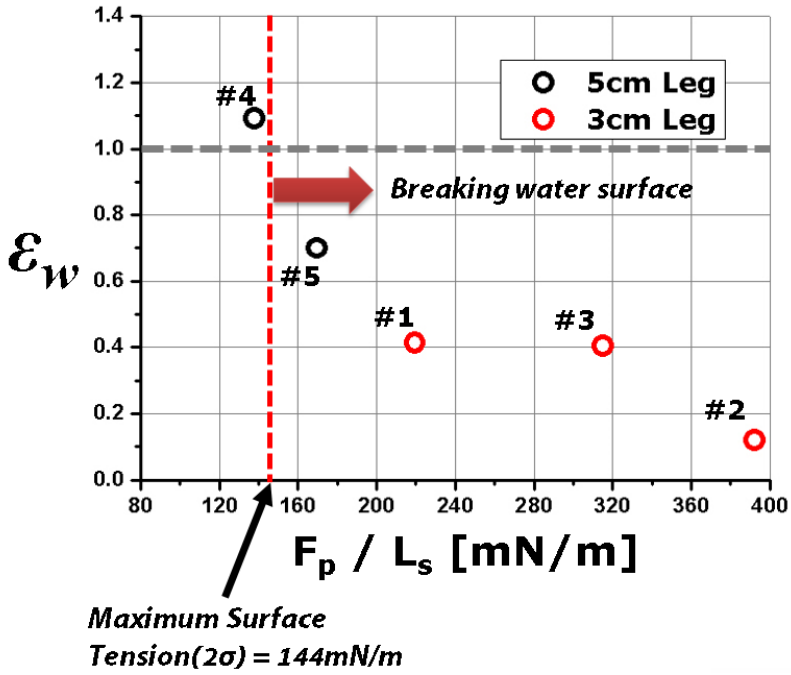

Figure IV. 30 Experimental results of the water-ground velocity ratio depending on different reaction force per submerged length

Surprisingly, the robot #4 has higher takeoff velocity on water than on rigid ground. By comparing jumping motion on water and ground, we can find the vibration magnitude of the legs is reduced when it jumps on water. Therefore, the mechanical efficiency of the jumping mechanism is increased when it jumps on water. The water effects to reduce the vibration of the legs. That causes the robot has a little bit higher takeoff velocity on water than jumping on ground.

Chapter V. Discussion and Conclusion

V.1 Strategy for Improving the Takeoff Velocity on Water

Based on this research, we are able to make the design strategy for improving the jumping performance on water in two directions depending on the maximum force of the robot as shown in Figure V. 1.

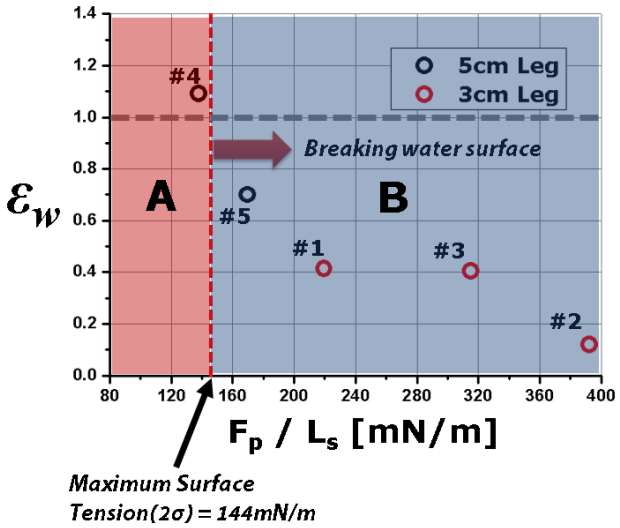

(a)

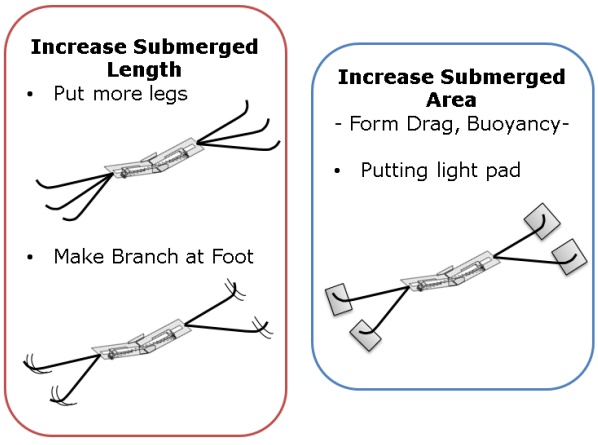

(b)

Figure V. 1 Design strategies for improving the jumping performance on water. (a) Two region divided by the maximum curvature force, (b) Two kinds of design modification strategies for improving the jumping performance on water

If the robot has lower driving force than the maximum curvature force as located in the region ‘A’ in Figure V. 1 (a), we should increase the submerged length for increasing the absolute value of the reaction force by putting more legs or some branches at the foot as shown in the red box of Figure V. 1 (b). With increasing the maximum reaction force, the robot can be designed to have much stronger actuator. Finally, the absolute value of the takeoff velocity would be improved.

At the other region ‘B’, the robot generates too high reaction force to use the curvature force. In that case, the takeoff velocity can be improved by using other hydrodynamic force such as drag, buoyancy and so on. In order to use the other forces, the submerged area of the foot should be considered significantly. Thin legs is hard to increase the drag, buoyancy, and inertia force because these forces has linear relationship with the area. Therefore, some pads can be put on the foot as shown in blue box of Figure V. 1 (b) for increasing the reaction force by using the drag, the buoyancy force and inertia force.

V.2 Conclusion and Future work

The real insect scale robotic water strider capable of jumping on water is developed by applying principles of the mechanism in the water strider locomotion. The hydrodynamics acting on the driving legs with the water surface is analyzed theoretically. By abstracting principles and criteria in order

to design the robotic water strider, the force profile generated by the robot is properly designed and finally the robotic water striders jump and leap out of the water surface smoothly without large splash as the real water striders do.

The hydrodynamic forces between the driving legs and the water surface is quantified theoretically with the parameters observed in advance. We found that the curvature force of the water surface is the largest and dominant hydrodynamic force in jumping on water of the water striders. The design criteria is established for the robot to obtain the maximum curvature forces from the water surface and not to break the water surface which causes reducing momentum transfer to the robotic water striders. The criteria is that the reaction force per submerged leg length should be below the maximum water surface curvature force generated by the surface tension of water. The principle guides for the robotic water striders to jump on water effective with the maximum momentum transfer.

To build the real scale robotic water strider, the manufacturing process and the materials used in the fabrication of the robotic water striders are carefully developed and selected with considering the scale and the efficiency. The real scale of the water striders is around the dimension of 2~3 cm in body length, 3~5 cm in leg length and weight of 50mg. It is much smaller and lighter than the conventional robotic systems and machines. Various conventional machining processes are inefficient for developing these meso-scale robotics systems. The robotic water striders weigh about 1/6 of a single 3mm nut which is basic element of conventional machines. To deal with manufacturing issues,

the smart composite microstructures (SCM) process is employed to build the small scale robotic structures. The precision laser machining and laminating process with fiber reinforced composite materials enable to fabricate millimeter scale articulated robotic structures with minimum friction loss in working. The fiber reinforce composites are light and strong compared to the metallic materials and those are suitable for miniaturization. The shape memory alloy (SMA) actuator is embedded on the robot as an artificial muscle of the robot. The high energy density and capability of large deformation in the SMA is superior characteristics for the small scale robots.

To satisfying the design criteria with maximum momentum transfer, the flea inspired catapult mechanism, called the torque reversal catapult, is employed to design the controllable jumping mechanism. The unique force profile generated by the torque reversal catapult mechanism enable to maximize the momentum transfer with the low reaction force. Moreover, the robot structure is simplified remarkably by applying the passive triggering components.

Finally, the robotic water strider prototypes are built with 2 cm in body length, 3~5cm in leg length and around 55 mg in weight. The robots can be designed with various design parameters to change the jumping power of the robots to meet the design criteria. The results show that the robotic water strider jumps and leaps out of the water surface smoothly with the takeoff velocity of 1.5 m/s. Surprisingly, if the robotic water strider satisfies the design criteria, the takeoff velocity on water and ground are almost same because the water surface

generate enough forces corresponding to the driving force of the legs. Water-ground velocity ratio from the experiments show the efficiency of jumping on water. When the reaction force per submerged length exceed the maximum curvature force of the water surface, the takeoff velocity on water decrease rapidly compared to the jumping on rigid ground.

By developing the robotic water strider, the robot itself would be used as an environment surveillance robots. In addition, the enabling technologies expand the scale limitation in the wide spectrum of robotics.

Bibliography

[1] K. Hirai, M. Hirose, Y. Haikawa, and T. Takenaka, "The development of Honda humanoid robot," in *1998 IEEE International Conference on Robotics and Automation, 1998. Proceedings* vol. 2, ed, 1998, pp. 1321-1326 vol.2.

[2] I.-W. Park, J.-Y. Kim, J. Lee, and J.-H. Oh, "Mechanical design of humanoid robot platform KHR-3 (KAIST Humanoid Robot 3: HUBO)," in *2005 5th IEEE-RAS International Conference on Humanoid Robots*, ed, 2005, pp. 321-326.

[3] U. Saranli, M. Buehler, and D. E. Koditschek, "RHex: A Simple and Highly Mobile Hexapod Robot," *The International Journal of Robotics Research,* vol. 20, pp. 616-631, 2001.

[4] S. Kim, J. E. Clark, and M. R. Cutkosky, "iSprawl: Design and tuning for high-speed autonomous open-loop running," *The International Journal of Robotics Research,* vol. 25, p. 903, 2006.

[5] P. Birkmeyer, K. Peterson, and R. S. Fearing, "DASH: A dynamic 16g hexapedal robot," in *IEEE/RSJ International Conference on Intelligent Robots and Systems, 2009. IROS 2009*, ed, 2009, pp. 2683-2689.

[6] R. J. Wood, "The First Takeoff of a Biologically Inspired At-Scale Robotic Insect," *Robotics, IEEE Transactions on,* vol. 24, pp. 341-347, 2008.

[7] K. Y. Ma, P. Chirarattananon, S. B. Fuller, and R. J. Wood, "Controlled flight of a biologically inspired, insect-scale robot," *Science,* vol. 340, pp. 603-7, May 3 2013.

[8] Y.-J. Park, U. Jeong, J. Lee, S.-R. Kwon, H.-Y. Kim, and K.-J. Cho, "Kinematic Condition for Maximizing the Thrust of a Robotic Fish Using a Compliant Caudal Fin," *IEEE Transactions on Robotics,* vol. 28, pp. 1216-1227, 2012.

[9] B. G. A. Lambrecht, A. D. Horchler, and R. D. Quinn, "A Small, Insect-Inspired Robot that Runs and Jumps," in *Proceedings of the 2005 IEEE International Conference on Robotics and Automation, 2005. ICRA 2005*,

ed, 2005, pp. 1240-1245.

[10] M. Kovac, M. Fuchs, A. Guignard, J. C. Zufferey, and D. Floreano, "A miniature 7g jumping robot," in *IEEE International Conference on Robotics and Automation, 2008. ICRA 2008*, ed, 2008, pp. 373-378.

[11] P. Fiorini and J. Burdick, "The Development of Hopping Capabilities for Small Robots," *Autonomous Robots,* vol. 14, pp. 239-254, 2003.

[12] M. Noh, S.-W. Kim, S. An, J.-S. Koh, and K.-J. Cho, "Flea-Inspired Catapult Mechanism for Miniature Jumping Robots," *IEEE Transactions on Robotics,* vol. 28, pp. 1007-1018, 2012.

[13] J.-s. Koh, S.-P. Jung, M. Noh, S.-W. Kim, and K.-j. Cho, "Flea inspired catapult mechanism with active energy storage and release for small scale jumping robot," in *2013 IEEE International Conference on Robotics and Automation (ICRA)*, ed, 2013, pp. 26-31.

[14] S. Kim, M. Spenko, S. Trujillo, B. Heyneman, D. Santos, and M. R. Cutkosky, "Smooth Vertical Surface Climbing With Directional Adhesion," *IEEE Transactions on Robotics,* vol. 24, pp. 65-74, 2008.

[15] M. W. Denny, *Air and Water: The Biology and Physics of Life's Media*: Princeton University Press, 1993.

[16] M. Dickinson, "Animal locomotion: How to walk on water," *Nature,* vol. 424, pp. 621-622 2003.

[17] D. L. Hu, B. Chan, and J. W. M. Bush, "The hydrodynamics of water strider locomotion," *Nature,* vol. 424, pp. 663-666 2003.

[18] J. W. M. Bush and D. L. Hu, "WALKING ON WATER: Biolocomotion at the Interface," *Annual Review of Fluid Mechanics,* vol. 38, pp. 339-369, 2006.

[19] X. Gao and L. Jiang, "Biophysics: Water-repellent legs of water striders," *Nature,* vol. 432, pp. 36-36 2004.

[20] X.-Q. Feng, X. Gao, Z. Wu, L. Jiang, and Q.-S. Zheng, "Superior Water Repellency of Water Strider Legs with Hierarchical Structures: Experiments and Analysis," *Langmuir,* vol. 23, pp. 4892-4896 2007.

[21] M. Burrows and G. P. Sutton, "Pygmy mole crickets jump from water," *Current Biology,* vol. 22, pp. R990-R991 2012.

[22] M. Burrows, "Jumping from the surface of water by the long-legged fly Hydrophorus (Diptera, Dolichopodidae)," *The Journal of Experimental Biology,* vol. 216, pp. 1973-1981, 2013.

[23] D.-G. Lee and H.-Y. Kim, "Impact of a Superhydrophobic Sphere onto Water," *Langmuir,* vol. 24, pp. 142-145, 2008.

[24] J.-s. Koh, S.-p. Jung, R. J. Wood, and K.-j. Cho, "A jumping robotic insect based on a torque reversal catapult mechanism," in *2013 IEEE/RSJ International Conference on Intelligent Robots and Systems (IROS)*, ed, 2013, pp. 3796-3801.

[25] G. P. Sutton and M. Burrows, "Biomechanics of jumping in the flea," *The Journal of Experimental Biology,* vol. 214, pp. 836-847, 2011.

[26] H. C. Bennet-Clark and E. C. A. Lucey, "The Jump of the Flea: A Study of the Energetics and a Model of the Mechanism," *Journal of Experimental Biology,* vol. 47, pp. 59-76, 1967.

[27] M. Rothschild, Y. Schlein, K. Parker, and S. Sternberg, "Jump of the Oriental Rat Flea Xenopsylla cheopis (Roths.)," *Nature,* vol. 239, pp. 45-48, 1972.

[28] M. Rothschild and J. Schlein, "Exoskeletal Structures and Musculature," *Philosophical Transactions of the Royal Society of London. B, Biological Sciences,* vol. 271, pp. 457-490, 1975.

[29] M. J. Cullen, "The Fine Structure of the Jumping Muscle," *Philosophical Transactions of the Royal Society of London. B, Biological Sciences,* vol. 271, pp. 491-497, 1975.

[30] M. Rothschild, J. Schlein, K. Parker, C. Neville, and S. Sternberg, "Execution of the Jump and Activity," *Philosophical Transactions of the Royal Society of London. B, Biological Sciences,* vol. 271, pp. 499-515, 1975.

[31] W. Gronenberg, "Fast actions in small animals: springs and click mechanisms," *Journal of Comparative Physiology A,* vol. 178, pp. 727-734, 1996.

[32] U. Scarfogliero, C. Stefanini, and P. Dario, "The use of compliant joints and elastic energy storage in bio-inspired legged robots," *Mechanism and Machine Theory,* vol. 44, pp. 580-590, 2009.

[33] A. Yamada, M. Watari, H. Mochiyama, and H. Fujimoto, "An asymmetric

robotic catapult based on the closed elastica for jumping robot," in *IEEE International Conference on Robotics and Automation, 2008. ICRA 2008*, ed, 2008, pp. 232-237.

[34] R. Armour, K. Paskins, A. Bowyer, J. Vincent, and W. Megill, "Jumping robots: a biomimetic solution to locomotion across rough terrain," *Bioinspiration & Biomimetics,* vol. 2, p. S65, 2007.

[35] J. Zhao, N. Xi, B. Gao, M. W. Mutka, and L. Xiao, "Development of a controllable and continuous jumping robot," in *2011 IEEE International Conference on Robotics and Automation (ICRA)*, ed, 2011, pp. 4614-4619.

[36] Y. Matsuyama and S. Hirai, "Analysis of Circular Robot Jumping by Body Deformation," in *2007 IEEE International Conference on Robotics and Automation*, ed, 2007, pp. 1968-1973.

[37] S. Bergbreiter and K. S. J. Pister, "Design of an Autonomous Jumping Microrobot," in *2007 IEEE International Conference on Robotics and Automation*, ed, 2007, pp. 447-453.

[38] R. J. Wood, S. Avadhanula, R. Sahai, E. Steltz, and R. S. Fearing, "Microrobot Design Using Fiber Reinforced Composites," *Journal of Mechanical Design,* vol. 130, pp. 052304-052304, 2008.

[39] J. P. Whitney, P. S. Sreetharan, K. Y. Ma, and R. J. Wood, "Pop-up book MEMS," *Journal of Micromechanics and Microengineering,* vol. 21, p. 115021, 2011.

[40] P. S. Sreetharan, J. P. Whitney, M. D. Strauss, and R. J. Wood, "Monolithic fabrication of millimeter-scale machines," *Journal of Micromechanics and Microengineering,* vol. 22, p. 055027, 2012.

[41] J.-S. Kim, D.-Y. Lee, J.-S. Koh, G.-P. Jung, and K.-J. Cho, "Component assembly with shape memory polymer fastener for microrobots," *Smart Materials and Structures,* vol. 23, p. 015011, 2014.

[42] J. Zhao, X. Zhang, N. Chen, and Q. Pan, "Why Superhydrophobicity Is Crucial for a Water-Jumping Microrobot? Experimental and Theoretical Investigations," *ACS Applied Materials & Interfaces,* vol. 4, pp. 3706-3711, 2012.

[43] *UltraTech International Inc.* http://www.spillcontainment.com/everdry.

[44] D. Vella, D.-G. Lee, and H.-Y. Kim, "The Load Supported by Small Floating Objects," *Langmuir,* vol. 22, pp. 5979-5981, 2006.

[45] D. Vella, "Floating Objects with Finite Resistance to Bending," *Langmuir,* vol. 24, pp. 8701-8706, 2008.

[46] F. M. White, *Fluid Mechanics*: McGraw-Hill, 2003.

국문 초록

소금쟁이 모사
초소형수면 도약 로봇

소금쟁이는 수면 위에서 미끄러지듯 걸어 다니며, 때로는 수면을 박차고 뛰어오르는 독특한 이동 능력을 가지고 있다. 수면 위를 쉽게 이동하는 소금쟁이의 운동 성능은 기존의 이동 로봇 또는 기계 시스템이 보여 줄 수 없었던 이동 능력이라 할 수 있다. 소금쟁이가 수면 위에서 보여 주는 뛰어나고 독특한 운동 능력은 초소형 수상 로봇의 개발에 있어 좋은 생체 모델이 될 수 있다. 이를 통해 로봇 제작 및 설계에 있어 크기 및 운동 능력의 한계를 뛰어 넘을 수 있는 기술 개발이 가능해 질 수 있는 것이다.

실제 곤충 크기의 소금쟁이 모사 수면 도약 로봇을 제작하기 위해서 소금쟁이의 운동 원리를 정확히 파악하여 로봇 설계의 기준을 확립 하였다. 소금쟁이가 도약 할 때 다리가 수면을 누르게 되며 다리와 수면 사이에서 다양한 유체역학적 (Hydrodynamic) 힘들이 발생하게 된다. 이들 중 물의 표면 장력에 의한 Curvature force 가 가장 큰 힘을 견디게 되고, 이는 다리가 수면을 깨뜨리지 않을 때에만 발생한다. 따라서 설계 기준은 수면을 깨뜨리지 않는 가장 큰 힘을 소금쟁이 로봇 다리에서 만들어 낼 수 있도록 설계하는 것으로 확립할

수 있다.

실제 소금쟁이는 2~3cm 크기며, 50mg 정도의 무게를 가지고 있다. 이러한 초소형, 초경량 스케일에서 로봇을 제작하기 위해 Smart Composite Microstructure (SCM) 제작 공정을 이용하여 복합재료와 고분자 필름 재료의 레이져 가공과 적층을 통해 로봇을 제작 하였다. 실제 로봇의 크기 또한 2cm 몸체와 60mg 의 무게로 실제 소금쟁이와 같은 스케일의 로봇을 제작 할 수 있었다. 그리고 필름 형태의 형상 기억 합금 구동기를 적용하여 초소형의 구동기를 만들 수 있었고, 이는 로봇 소형화의 핵심적인 역할을 하였다.

설계 기준을 만족 시키며 최대한 도약 성능을 높이기 위해서는 수면을 깨뜨리지 않는 힘으로 운동량을 최대화 시키는 메커니즘 설계가 필요하다. 이를 위해 본 연구에서는 초소형 도약 곤충인 벼룩의 다리 구조에서 착안한 토크 역전 메커니즘을 적용하였다. 이는 낮은 힘을 유지하며 서서히 몸체의 속도를 증가시키는 특성을 가지고 있어, 소금쟁이 로봇에 적용할 경우 수면을 깨뜨리지 않는 힘으로 높은 도약 속도를 얻을 수 있다.

로봇 다리가 내는 힘을 정밀하게 예측하기 위해 로봇의 동역학 모델을 확립하여 지상에서 그리고 수면에서 로봇이 받을 수 있는 힘을 다양한 디자인 변수에 따라 시뮬레이션 할 수 있었다. 소금쟁이 로봇의 다리 길이, 구동기의 강성을 다르게 하여 로봇의 반작용력을

예측하고, 설계 기준을 만족시키는 로봇을 설계할 수 있었다.

도약 실험을 통해 로봇의 설계 기준을 증명할 수 있었다. 1.5 m/s의 도약 속도는 실제 소금쟁이의 성능과 유사한 수치이며, 독특한 점은 지상에서와 수면에서 도약 속도가 크게 차이가 없다는 것이다. 이는 수면에서도 지상에서와 같이 충분한 힘을 얻을 수 있어서 가능하였다고 할 수 있다.

소금쟁이 모사 수면 도약 로봇 개발을 통해 앞으로 초소형 로봇 개발의 기반 기술로 사용될 수 있을 것으로 기대하며, 초소형 소금쟁이 로봇은 미래의 수상 환경 감시, 군사용 정보 획득에 사용되는 초소형 로봇 플랫폼이 될 수 있을 것이다.